

Lattice Dynamics of $\text{YBa}_2\text{Cu}_3\text{O}_{6+x}$ ($x = 0.25, 0.5, 0.75$)

K. K. Yim,^A J. Oitmaa^A and M. M. Elcombe^B

^A School of Physics, University of New South Wales,
Kensington, PO Box 1, N.S.W. 2033, Australia.

^B Australian Nuclear Science and Technology Organisation,
Menai, N.S.W. 2234, Australia.

Abstract

The lattice dynamics of $\text{YBa}_2\text{Cu}_3\text{O}_{6+x}$ with partially filled O(4) sites is investigated using a supercell method. The model used is the lattice-dynamical shell model, which incorporates the short-range interactions and the long-range Coulomb potential as well as the polarisabilities of ions. Varying the oxygen content produces small changes throughout the spectrum of normal modes, as well as major changes in those modes with large O(4) amplitudes. Selected phonon dispersion curves are presented, with emphasis on the variation of frequency with oxygen concentration. The nature of new modes, which appear with an increase in oxygen concentration, is investigated. The overall phonon density of states is also presented.

1. Introduction

Since the discovery of high- T_c superconductivity in the Y–Ba–Cu–O materials, the lattice dynamics of both the superconducting $\text{YBa}_2\text{Cu}_3\text{O}_7$ and semiconducting $\text{YBa}_2\text{Cu}_3\text{O}_6$ have been the focus of much work. Many experiments using Raman scattering (e.g. McCarty *et al.* 1990) and infrared absorption (e.g. Genzel *et al.* 1989) have been carried out to probe the $\mathbf{k} = 0$ modes of these systems. Neutron scattering methods have been used to measure the phonon density of states (Renker *et al.* 1988*a*, 1988*b*) and phonon dispersion curves (Pintschovius 1990; Pintschovius *et al.* 1991). Lattice-dynamical model calculations have been reported by many workers (Kress *et al.* 1988; Yasuda and Mase 1989; Yim *et al.* 1992). Much of the early work has been reviewed by Feile (1989).

To date, theoretical calculations have considered only the limiting structures, *viz.* $x = 0$ and $x = 1$. Most experimental studies have also focused on these two structures, or other structures with x values close to them, since the oxygen concentration and distribution cannot be monitored precisely. However, there is also considerable interest in intermediate values of the oxygen concentration, $0 < x < 1$. For example, it is well known that the curve of the superconducting transition temperature T_c versus x shows a plateau at $x \approx 0.5$, and it has been conjectured that this is related to the oxygen ordering in the O(4) sites. (See Fig. 1 for the ion labelling.) Experiments have revealed the possible existence of a number of stable ordered phases (Van Tendeloo *et al.* 1987; Zeiske *et al.* 1992) and these have been extensively modelled using phenomenological lattice–gas models (de Fontaine *et al.* 1987; Aukrust *et al.* 1990; Burdett 1992; Aligia *et al.* 1992).

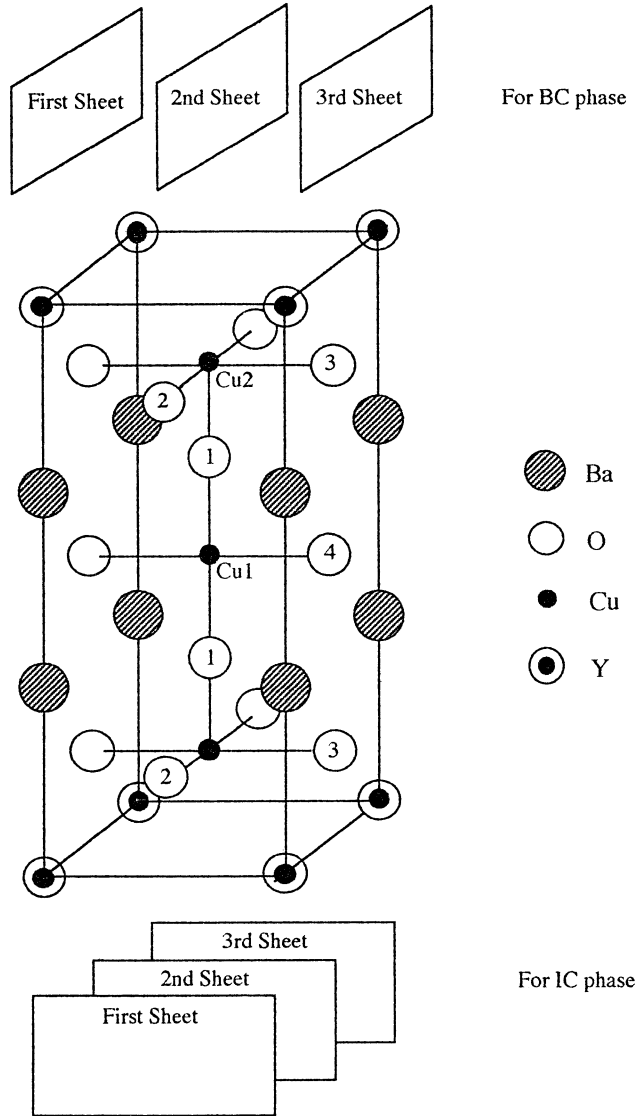


Fig. 1. Conventional unit cell of $\text{YBa}_2\text{Cu}_3\text{O}_7$. Also shown are the vertical sheets of ions in the cell.

Some Raman and infrared studies have also been performed on $\text{YBa}_2\text{Cu}_3\text{O}_{6+x}$ with intermediate values of x (e.g. Blumberg *et al.* 1989; Burns *et al.* 1991; Echegut *et al.* 1989; Crawford *et al.* 1988; Morioka *et al.* 1989). The behaviour of the $\mathbf{k} = 0$ normal modes with respect to oxygen content, in particular the A_g Raman modes, has been studied rather thoroughly. The frequencies and intensities of some modes are found to vary considerably with oxygen content. Nevertheless, the experimental work for intermediate x is less comprehensive than that for the two limiting structures. Moreover, no theoretical studies have been reported on the lattice dynamics of the intermediate- x materials.

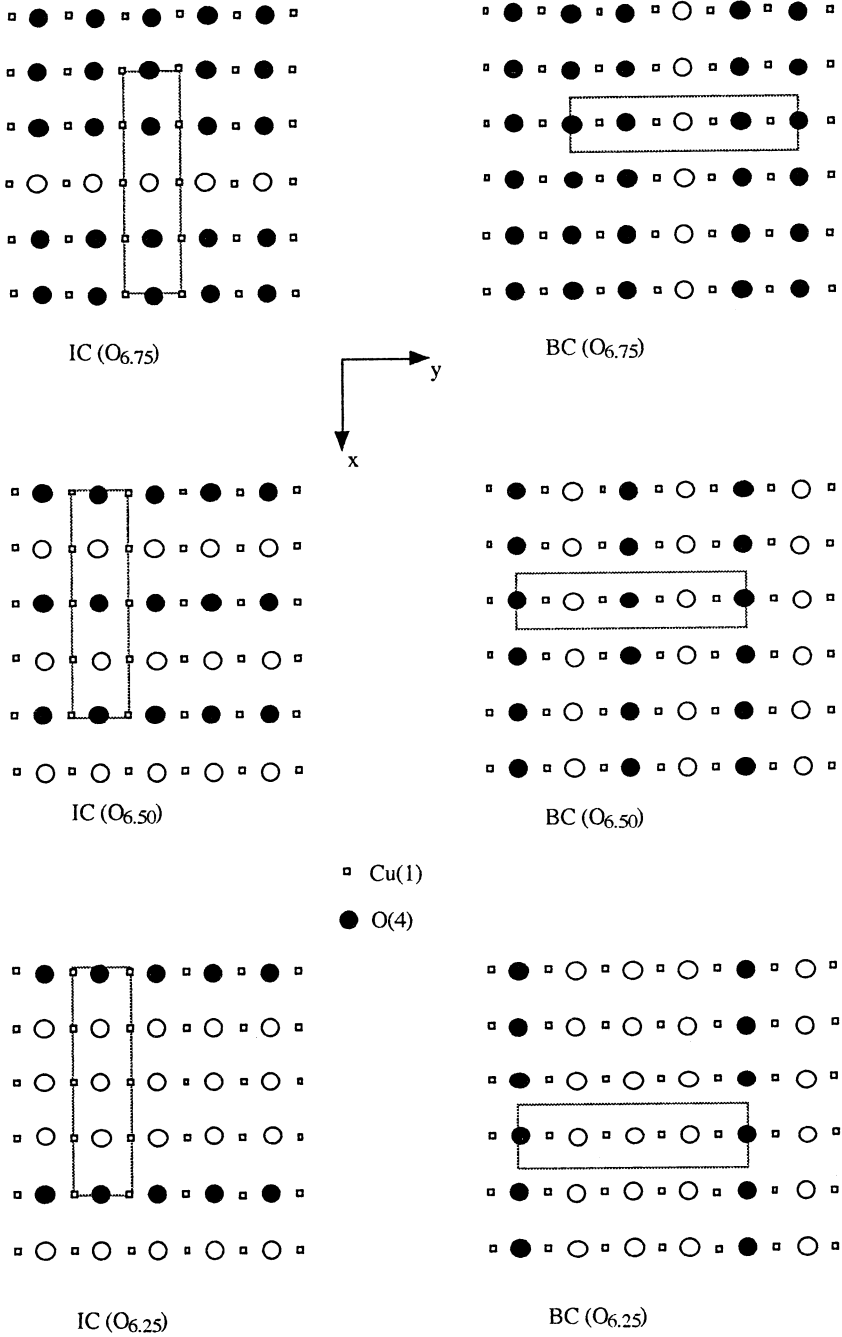


Fig. 2. Structures of the IC and BC phases, showing the plane of the Cu–O chains. The filled circles represent the filled O(4) sites, while the open circles represent vacancy sites. The rectangles represent the supercells.

Motivated by this, we have undertaken a series of theoretical studies of the lattice vibrations in the $\text{YBa}_2\text{Cu}_3\text{O}_{6+x}$ systems with intermediate oxygen concentrations. An immediate difficulty is that in the real systems the distribution of oxygens will certainly be non-uniform, and hence impossible to model. In our calculations we must assume that the oxygen distribution is uniform and periodic in the Cu(1)–O(4) chain, allowing the use of a large unit cell, or ‘supercell’, which is repeated periodically. In addition we ignore any possible vacancies forming in other oxygen sites (Jorgensen *et al.* 1990). While this makes comparison with the existing experimental results difficult, we believe that our results, and particularly the trends observed with a variation of x , are useful for understanding these materials.

2. Model and Method

Methods

In the study of non-stoichiometric crystals, two different approaches are available. One is the mean-field or ‘effective-atom’ approach, in which the site with fractional occupation is treated as having a fictitious atom of reduced mass and force constants in every unit cell in the whole crystal. In our case this means that all the O(4) sites along the Cu(1)–O(4) chains are occupied by fictitious atoms. The strengths of interaction between the fictitious oxygen and other constituents of the crystal are scaled from the full strengths by a factor related to the occupation probability of the sites. Such a mean-field approach, though it will almost certainly give a good qualitative description of the system, has one serious shortfall—it blurs out any ordering of the fractionally occupied sites, which might otherwise exist in the system. Hence, no information on properties related to the ordering can be unambiguously obtained using this method. Since there is at least partial ordering of oxygens in the Cu–O chains of $\text{YBa}_2\text{Cu}_3\text{O}_{6+x}$, except at very high temperature, the mean-field approach will not be so appropriate.

The alternative approach is the supercell method, which we employ in our present work. In this method, instead of considering fictitious atoms in every single unit cell, a number of unit cells are taken to form a supercell with some unfilled oxygen sites along the chain. Thus we can consider structures with different oxygen stoichiometries and ordering, provided they possess some overall periodicity. In the present paper we study structures with $x = 0, 0.25, 0.50, 0.75$ and 1.00 . For each value of x , two phases are investigated: the intact chain phase and the broken chain phase, designated IC and BC phases respectively. To form the fractional x structures in the IC phases, complete chains of O(4) oxygens are removed, while in the BC phases the Cu–O chains are broken by removing selected O(4) oxygens within every chain (see Fig. 2 for their structures). The space group symmetry of all the structures with fractional x is $D_{2h}^1(Pmmm)$.

Calculation

To study systems with $x = 0.25$ and 0.75 we require a supercell which is four times the size of the conventional unit cell. This is the minimum size for the supercell for which the above two systems can be modelled. For the IC phases this supercell takes the form $(4a \times 1b \times 1c)$, where a, b, c represent the usual lattice parameters. For the BC phases the supercell has the form $(1a \times 4b \times 1c)$.

For $x = 0.5$ a supercell of the form $(2a \times 1b \times 1c)$ or $(1a \times 2b \times 1c)$ could be used. However, to compare the calculated phonon dispersion curves for different values of x , it is most convenient to use the same supercell for all x . Thus in this manner (with reference to Fig. 2) the supercells for $x = 0.25, 0.75$ are by themselves primitive unit cells but the supercells for $x = 0, 0.50$ and 1.0 are non-primitive unit cells. There are four primitive unit cells in the supercells for $x = 0, 1.0$ and two primitive unit cells for $x = 0.50$.

Since the number of ions in a unit cell has now increased (48 for $x = 0$ to 52 for $x = 1$, compared with 12 and 13 for the corresponding x in the conventional unit cell), the size of the dynamical matrix is now much greater. This does not pose a serious problem because many of the matrix elements are related by symmetry even for fractional- x structures. However, the number of phonon modes at each \mathbf{q} has increased fourfold. This complicates the analysis and the comparison between phonon structures of different x .

The new Brillouin zone is four times smaller than the conventional one. It can be obtained by folding the conventional Brillouin zone in the same direction as that in which the unit cell is increased. This is illustrated in the Appendix in terms of a two-dimensional model. A consequence of this folding is that different \mathbf{q} values in the original Brillouin zone, and the phonon modes belonging to these \mathbf{q} , are mapped onto the same point in the reduced Brillouin zone. This folding generates some symmetry-related problems. For $x = 0.25$ and 0.75 the supercells are primitive and their Brillouin zones are the conventional ones. Hence for these two structures the symmetries of all the phonon modes of any interior \mathbf{q} point in the Brillouin zone are unique, and only the symmetries of the zone-boundary modes are origin-dependent (Cornwell 1971). However, for $x = 0, 0.5, 1.0$, the supercells are non-primitive and their Brillouin zones are the reduced ones. Some of the zone-boundary modes from the conventional Brillouin zone are mapped onto the interior of the reduced Brillouin zone. The symmetry classification for these zone-boundary modes are origin-dependent, irrespective of their positions in the reduced Brillouin zone and the choice of the unit cell.

In our calculations the choice of the origin is the O(4) sites because these positions possess the full point group symmetry for each value of x . For $x = 0$ and 1.0 all the O(4) sites are equivalent because for $x = 0$ they are all vacant and for $x = 1.0$ they are all filled. Hence choosing the origin at any of the O(4) sites will give the same symmetry classification for the phonon modes of any \mathbf{q} . For $x = 0.50$ the origin can be on a filled O(4) site or on a vacant O(4) site. These choices will result in a different symmetry classification for phonon modes originating from the zone boundary. The complete set of dispersion curves is however, independent of the choice of origin.

Model

The lattice-dynamical model that we use is the well-known shell model. It incorporates short-range overlap forces, long-range Coulomb forces and the polarisabilities of ions in the crystal lattice. The polarisability of an ion is related to the shell charges and core-shell spring constants of the ions. A detailed description of the form of shell model we are using can be found in our previous work (Yim *et al.* 1992). We do not include screening in the present model as we

found previously that even for the $\text{YBa}_2\text{Cu}_3\text{O}_7$ system a reasonable description is possible without screening.

Table 1. Selected shell-model parameters for $\text{YBa}_2\text{Cu}_3\text{O}_6$ and $\text{YBa}_2\text{Cu}_3\text{O}_7$

Only parameters which are different from those in our previous work (Yim *et al.* 1992) are tabulated. For $\text{YBa}_2\text{Cu}_3\text{O}_6$ the unchanged parameters correspond to those of Model 1 and for $\text{YBa}_2\text{Cu}_3\text{O}_7$ those of the unscreened shell-model (Model 2) in our previous work.

$\text{YBa}_2\text{Cu}_3\text{O}_6$		Shell charges (e)	
Ions		Previous	New
Cu(1)		4.48	3.68
O(1)		-3.24	-3.00

$\text{YBa}_2\text{Cu}_3\text{O}_7$		Ionic charges (e)	
Ions		Previous	New
Ba		1.85	1.775
O(2,3)		-1.80	-1.775
O(4)		-1.65	-1.600

$\text{YBa}_2\text{Cu}_3\text{O}_7$	Core-shell spring constants (e^2/v_a) (k_{perp} k_{bond} k_z)			
	Previous		New	
O(4)	(496	1003	496)	(396 unchanged 396)

$\text{YBa}_2\text{Cu}_3\text{O}_7$	Short-range force constants ($e^2/2v_a$)			
	Previous		New	
Ions-Ions	A	B	A	A
Cu(1)-O(4)	350.0	-40.0	Unchanged	-20.0
O(1)-O(4)	-5.5	4.0	Unchanged	5.0
Ba-O(1)	90.5	-6.0	89.0	-7.0

The shell-model parameters that we use in our present work are based on those obtained previously (Yim *et al.* 1992) using a least-squares fitting to the inelastic neutron data for $\text{YBa}_2\text{Cu}_3\text{O}_6$ (Pintschovius 1990; Pintschovius *et al.* 1991). Our initial parameter set for the two limiting structures of $\text{YBa}_2\text{Cu}_3\text{O}_{6+x}$ ($x = 0, 1$) was that of Model 1 in our previous paper. However, for the present work some fine tuning of these parameter values is necessary in order that the parameter sets of the fractional- x structures, which are obtained via a consistent interpolation scheme, are free from phonon instabilities. The $x = 0.25$ structures seem particularly prone to instabilities. The adjustments to the model parameters are given in Table 1. We retain as many as possible of the model parameters of the previous work, especially for $\text{YBa}_2\text{Cu}_3\text{O}_6$, because they were obtained on the basis of a systematic least-squares analysis. The major changes in the parameters are those of the Cu(1)-O(4) chain, as one would have expected, since this part of the crystal is changing as we vary x . The new magnitudes of the shell charges of Cu(1) and O(1) for $\text{YBa}_2\text{Cu}_3\text{O}_6$ have been reduced considerably in comparison with their initial values. Other modifications to the parameters, in

particular those of O(2) and O(3) in $\text{YBa}_2\text{Cu}_3\text{O}_7$, are necessary to balance the changes in the parameters of O(4) in order to maintain a reasonably good fit to the experimental phonon data of $\text{YBa}_2\text{Cu}_3\text{O}_7$ (Pintschovius 1990; Pintschovius *et al.* 1991).

In the calculations for other values of x ($= 0.25, 0.50$ and 0.75) the short-range force constants, the shell charges and the core-shell spring constants are interpolated from those of the two limiting structures ($x = 0, 1$) on the assumption that they vary linearly with the oxygen content. The lattice constants a, b, c and the atomic positions of the ions in these structures are also obtained through linear interpolation. In doing so we have ignored the structural anomalies (Cava *et al.* 1990) at $0.30 < x < 0.45$, which would require an equally abrupt change to the model parameters and would further complicate the calculations. Phases with $x \leq 0.5$ are assumed to have a tetragonal structure in which the average of a and b is used as the single-cell lattice parameters for the x and y directions. The corresponding atomic coordinates, short-range force constants and the core-shell spring constants are also averaged in this way.

The problem of ionic charges in the non-stoichiometric systems is more complicated. We need a method of varying the ionic charges systematically in response to oxygen removal, which at the same time can fulfil the requirement of charge neutrality. The way we resolve this is by considering the Y-Ba-Cu-O crystal to be made of vertical sheets of ions (see Fig. 1). The sheets are parallel to the Cu(1)-O(4) chains in the IC phases and perpendicular in the BC phases. If a sheet has the environment of $\text{YBa}_2\text{Cu}_3\text{O}_7$ then we assign the charges of ions on the sheet with the ionic charges of $\text{YBa}_2\text{Cu}_3\text{O}_7$, and likewise for the $\text{YBa}_2\text{Cu}_3\text{O}_6$ environment. However, if the sheet is in an environment intermediate between $\text{YBa}_2\text{Cu}_3\text{O}_7$ and $\text{YBa}_2\text{Cu}_3\text{O}_6$, then an ion on the sheet will take the average ionic charge of the two. In this way the charge neutrality requirement will always be maintained.

3. Results and Discussion

The model and method described above were used to determine the phonon dispersion curves for $x = 0, 0.25, 0.50, 0.75$ and 1.00 for both the IC and BC phases. The overall results are shown in Figs 3–6. Fig. 3 shows the dispersion curves for the IC phase with \mathbf{q} in the [100] direction. The phonon modes are classified according to their symmetries. Note that for $x = 0, 0.5$ and 1.0 there are degeneracies within the Brillouin zone due to crossing of dispersion curves. This is due to the folding of the original Brillouin zone (see the Appendix). For the same reason degeneracies exist at the zone centre and the zone boundary for $x = 0$ and 1.0 . These degeneracies are lifted for $x = 0.25, 0.75$ —for in these cases the Brillouin zone is the primitive one. Fig. 4 shows similar results for the BC phase with \mathbf{q} in the [010] direction. Fig. 5 gives the dispersion curves for the IC phase with \mathbf{q} in the [001] direction. In this direction two sets of dispersion curves (labelled V and F) are presented for $x = 0.50$ because the symmetry classification of some phonon modes is now dependent on the choice of origin as discussed earlier. The set V is obtained with the origin at a vacant O(4) site, while the set F is obtained with the origin at a filled site. Fig. 6 shows similar results for the BC phase, with \mathbf{q} in the [100] direction. Note that for Figs 3 and 4 the dispersion curves are folded onto themselves (self-folding), but for Figs 5 and 6 this is no longer the case (see the Appendix).

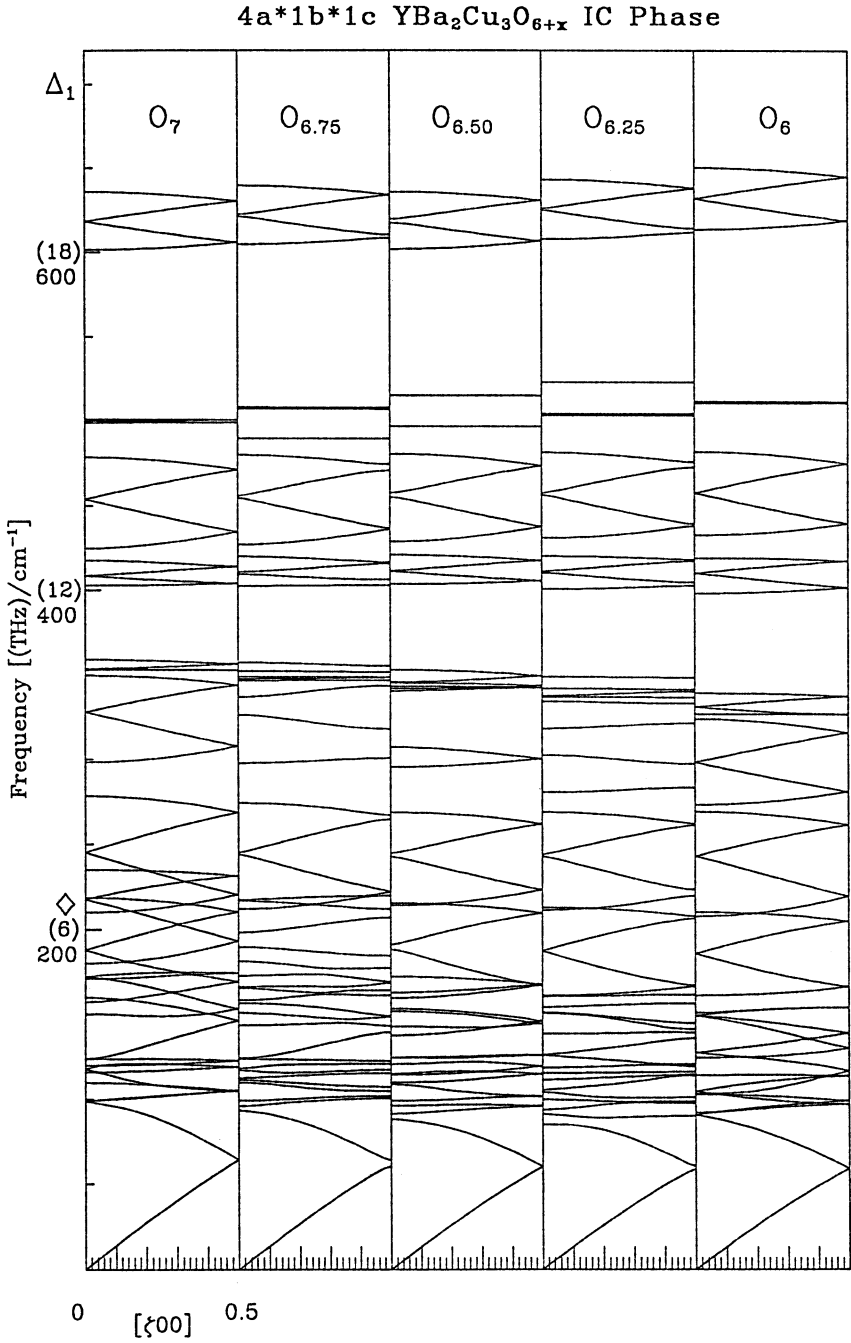


Fig. 3. Dispersion curves of YBa₂Cu₃O_{6+x} for IC phase with q in the [100] direction. The diamond indicates the disappearance of branches.

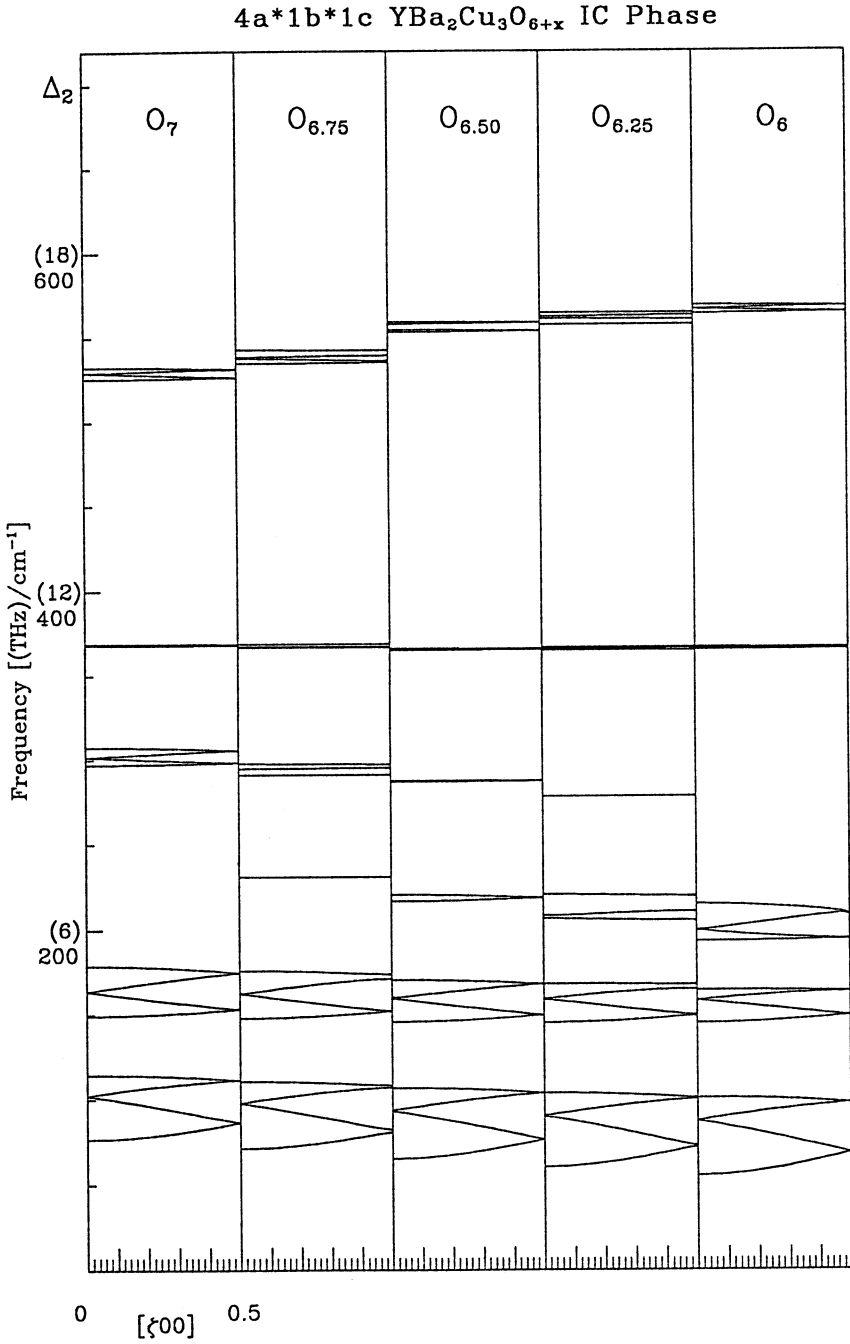


Fig. 3b

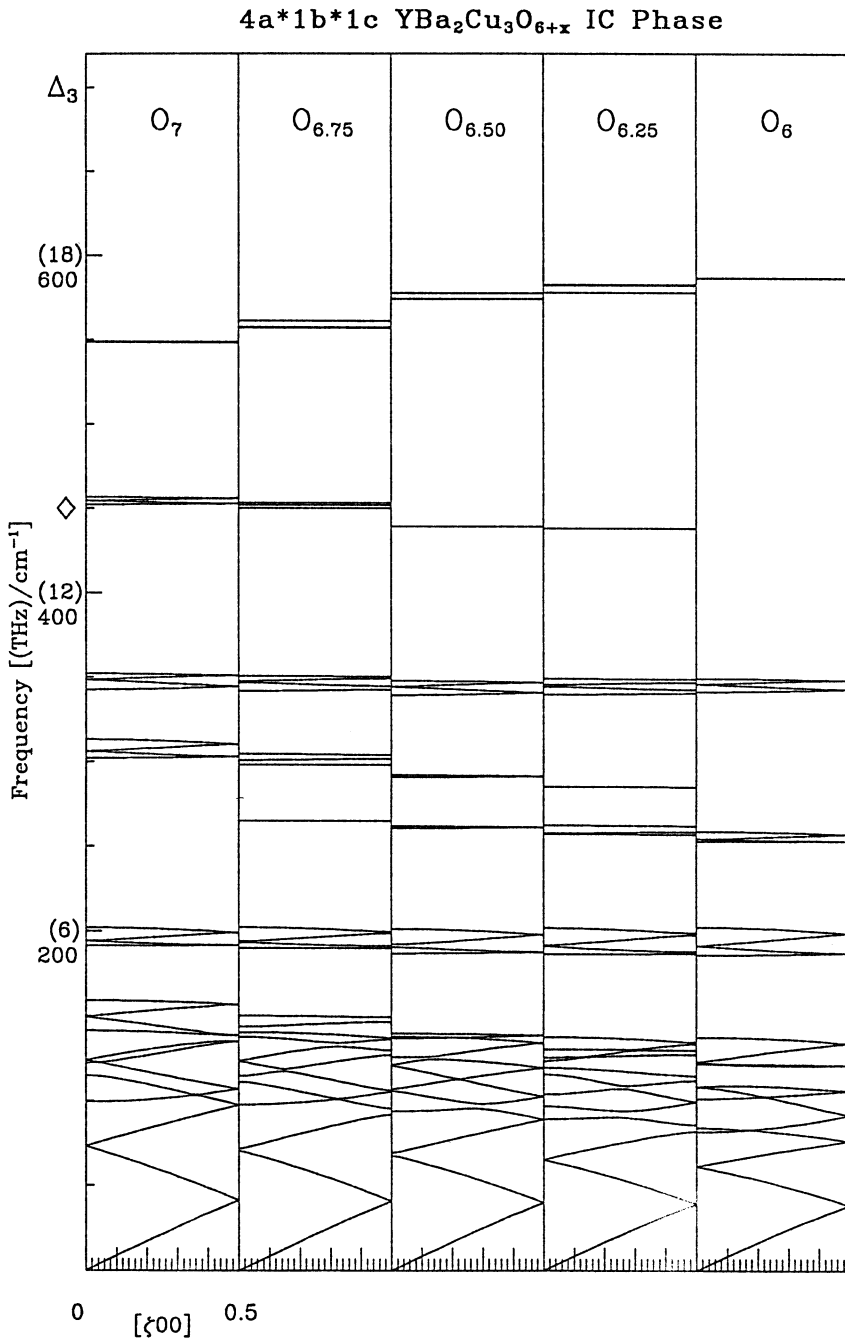


Fig. 3c

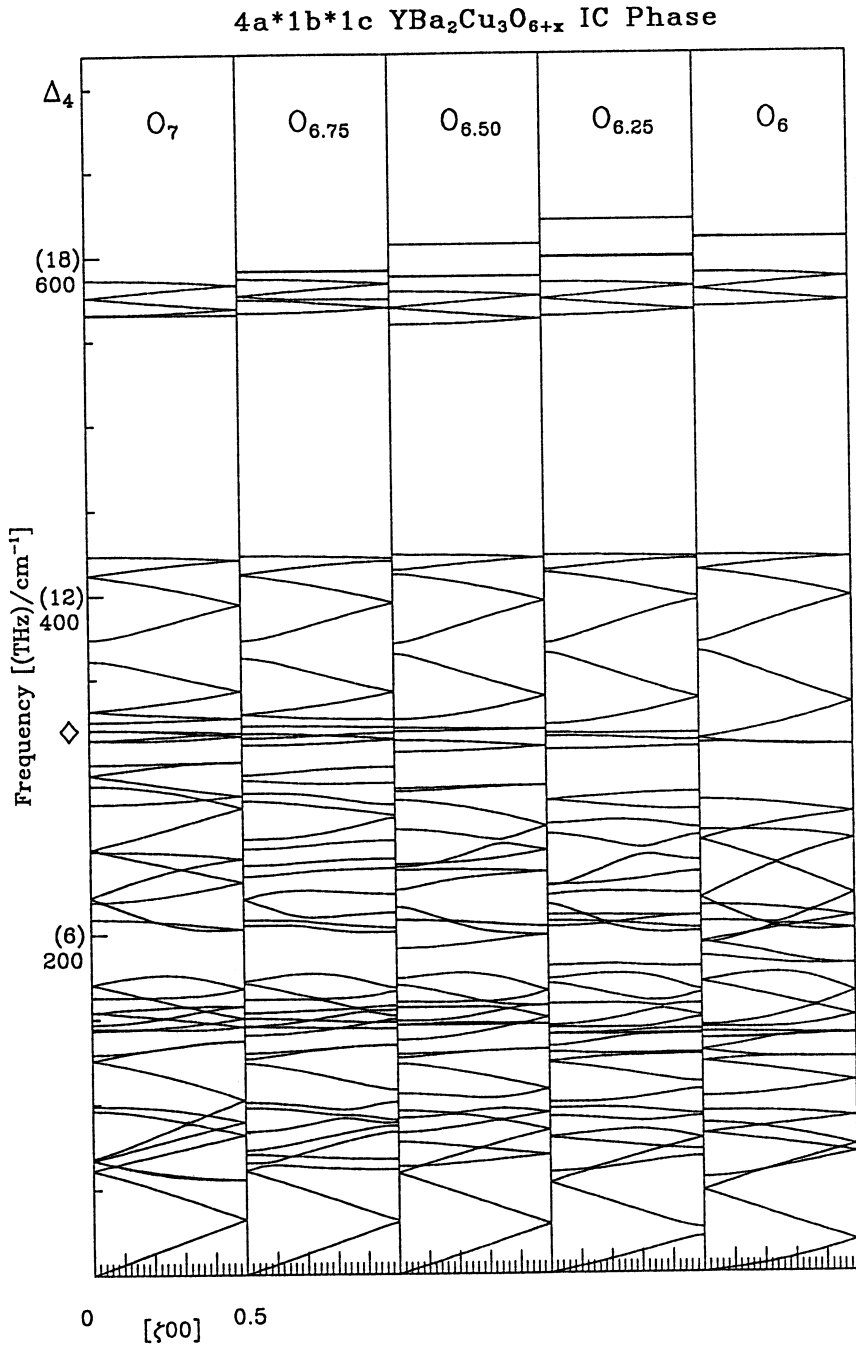


Fig. 3d

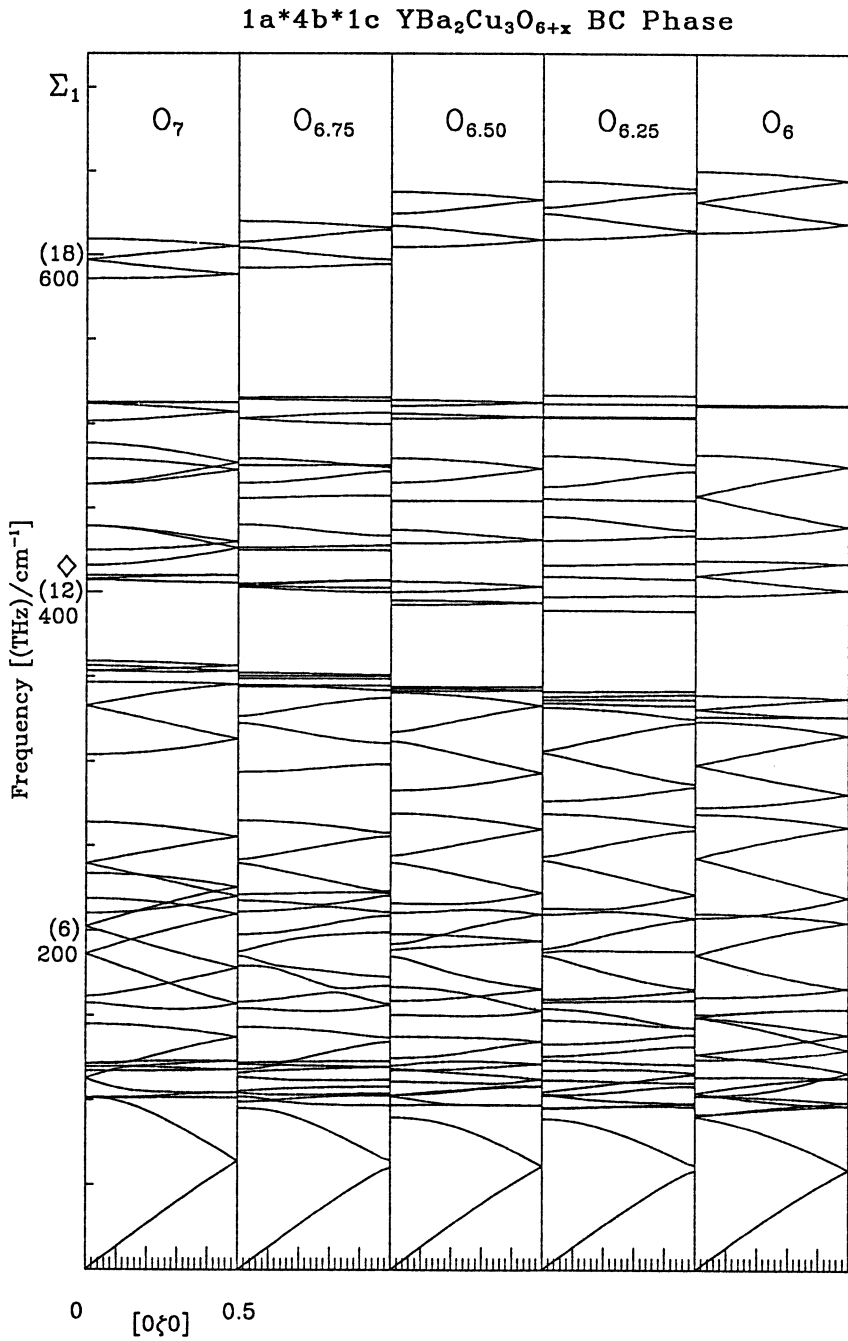


Fig. 4. Dispersion curves of YBa₂Cu₃O_{6+x} for BC phase with q in the [010] direction. The diamond indicates the disappearance of branches.

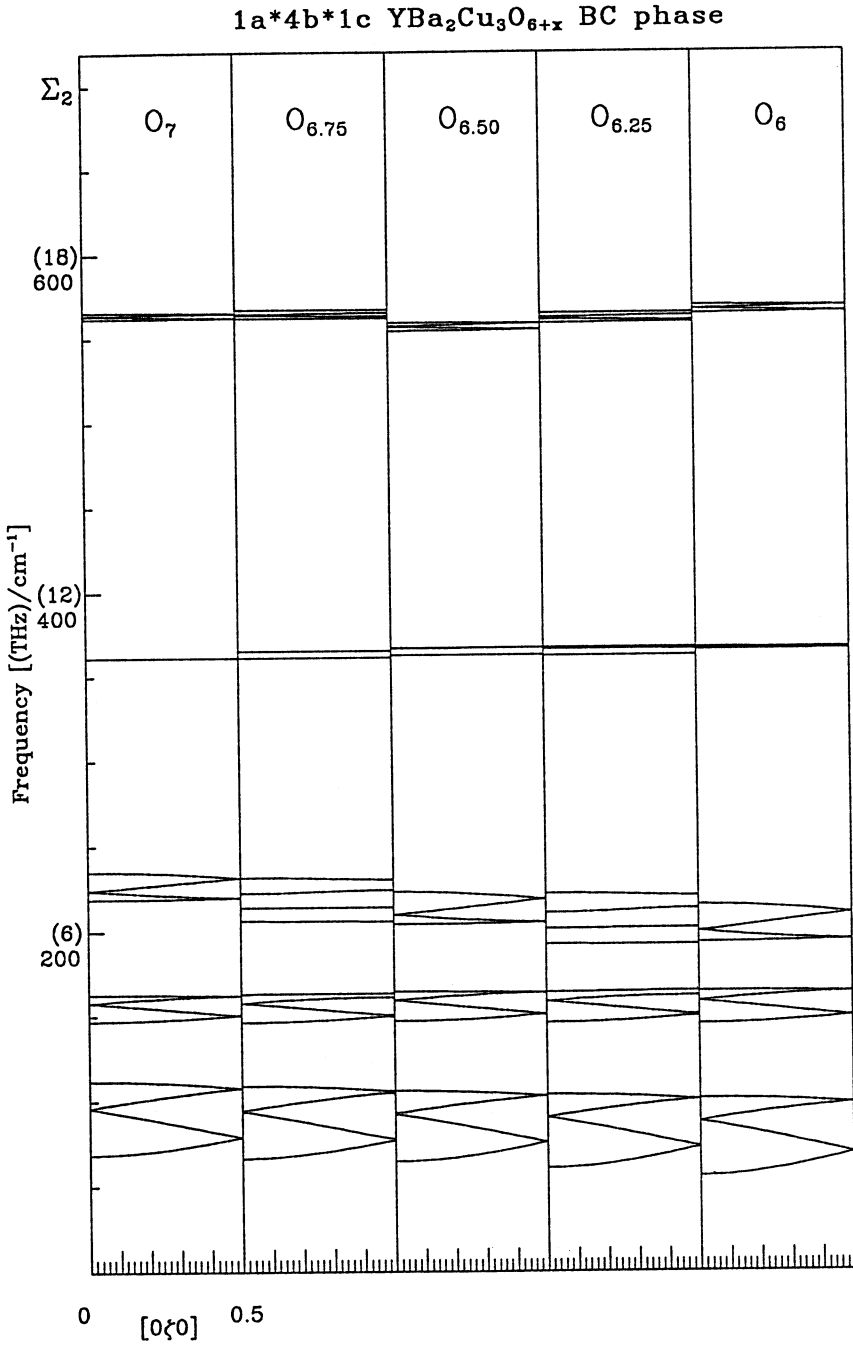


Fig. 4b

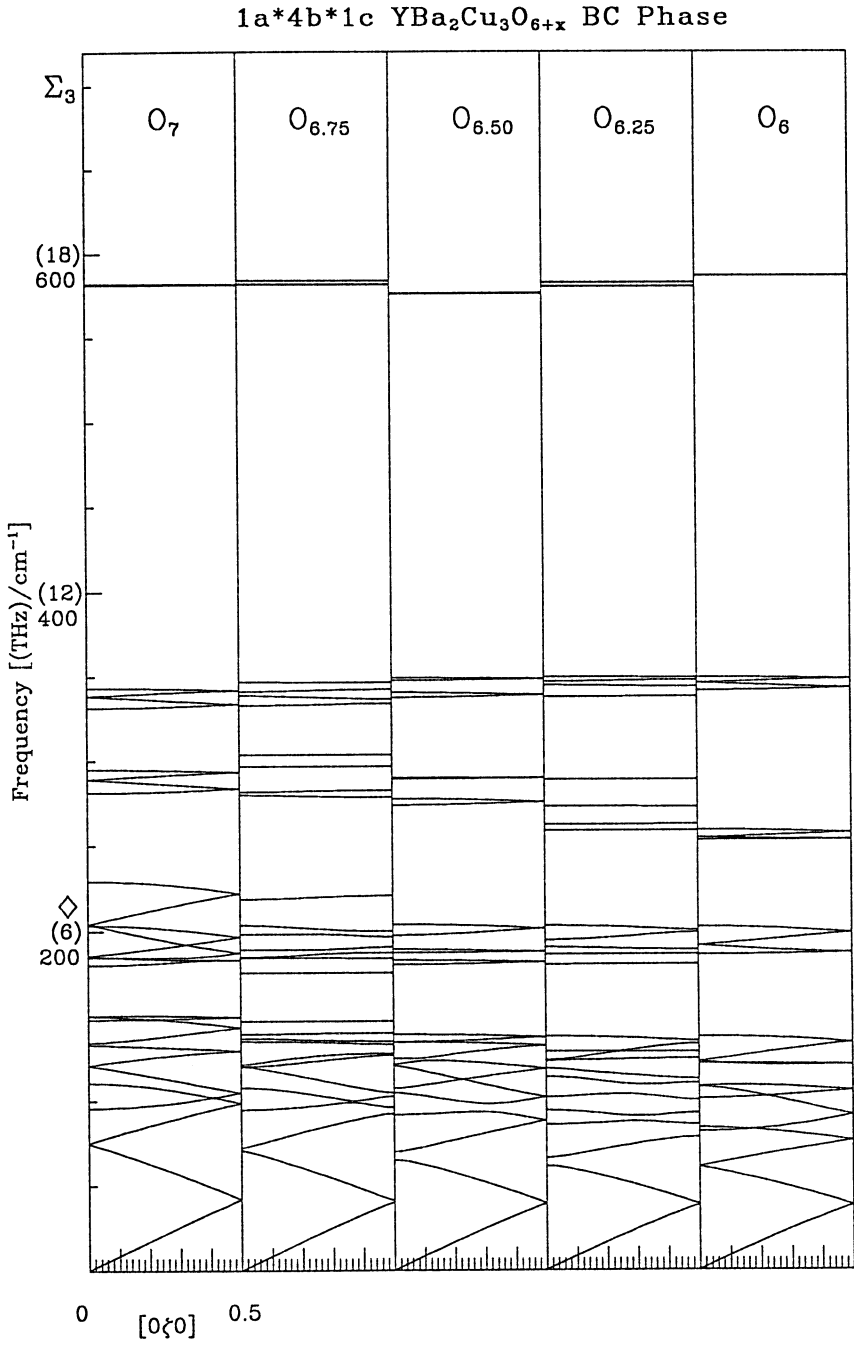


Fig. 4c

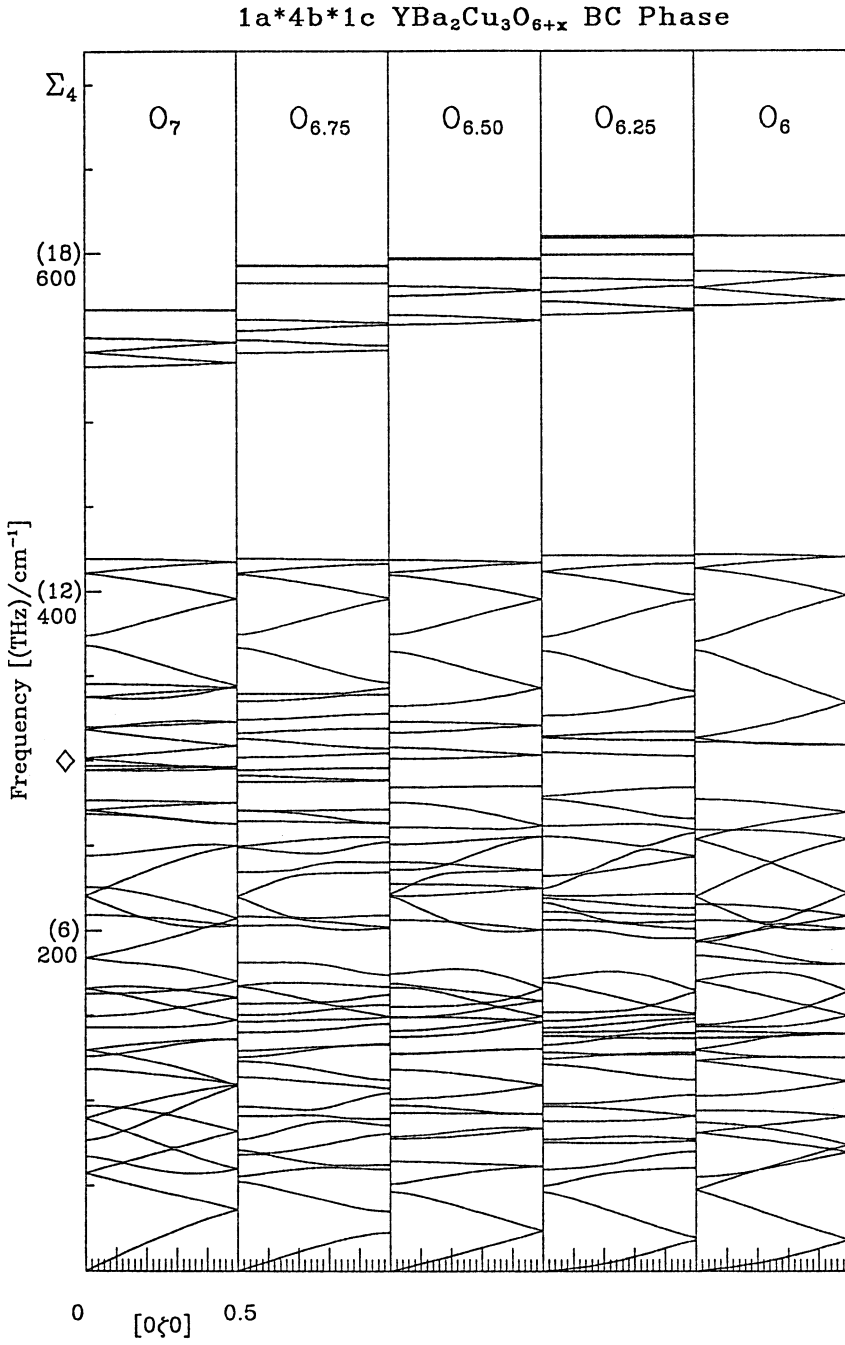


Fig. 4d

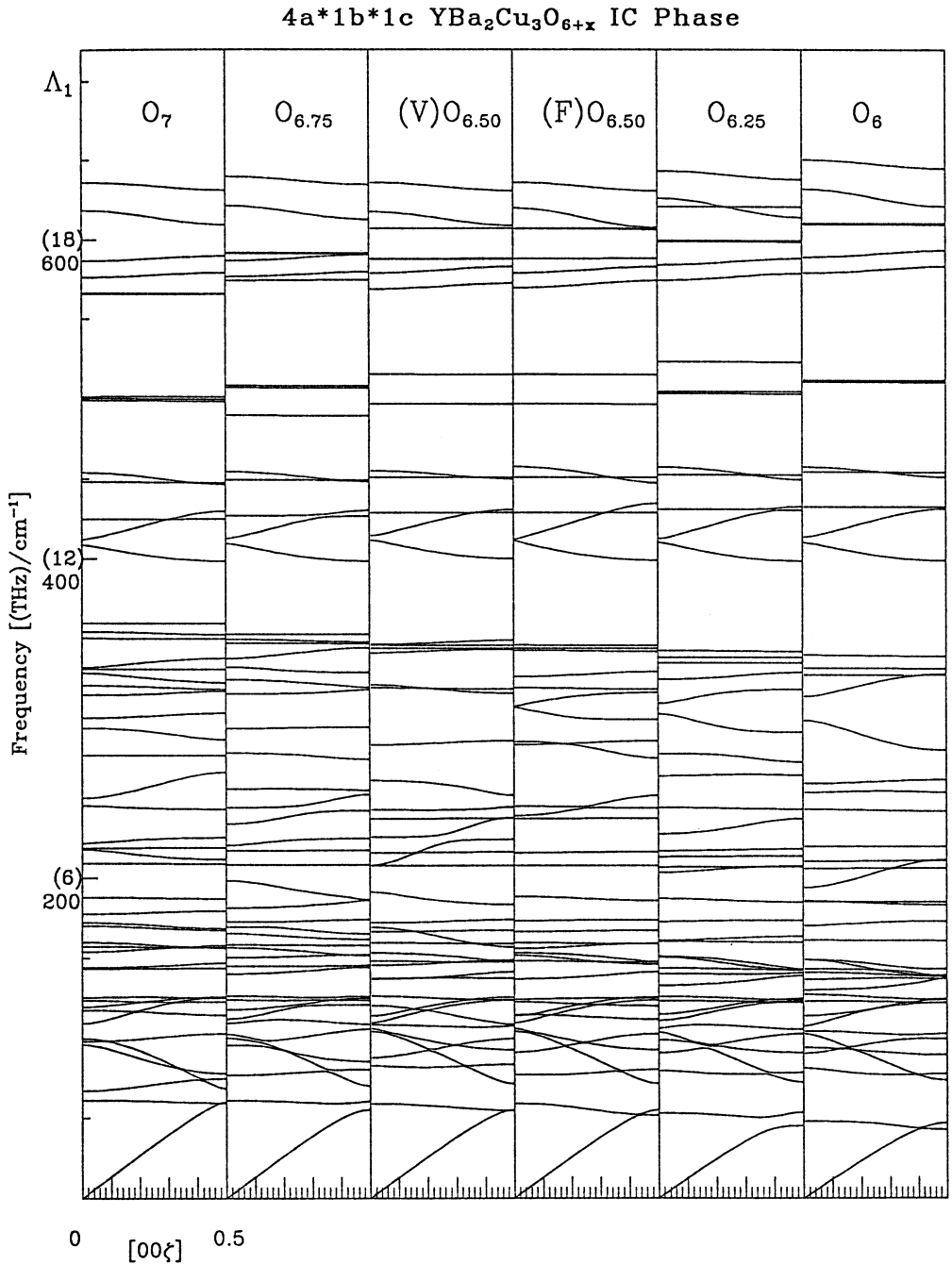


Fig. 5. Dispersion curves of $\text{YBa}_2\text{Cu}_3\text{O}_{6+x}$ for IC phase with q in the $[001]$ direction. The diamond indicates the disappearance of branches.

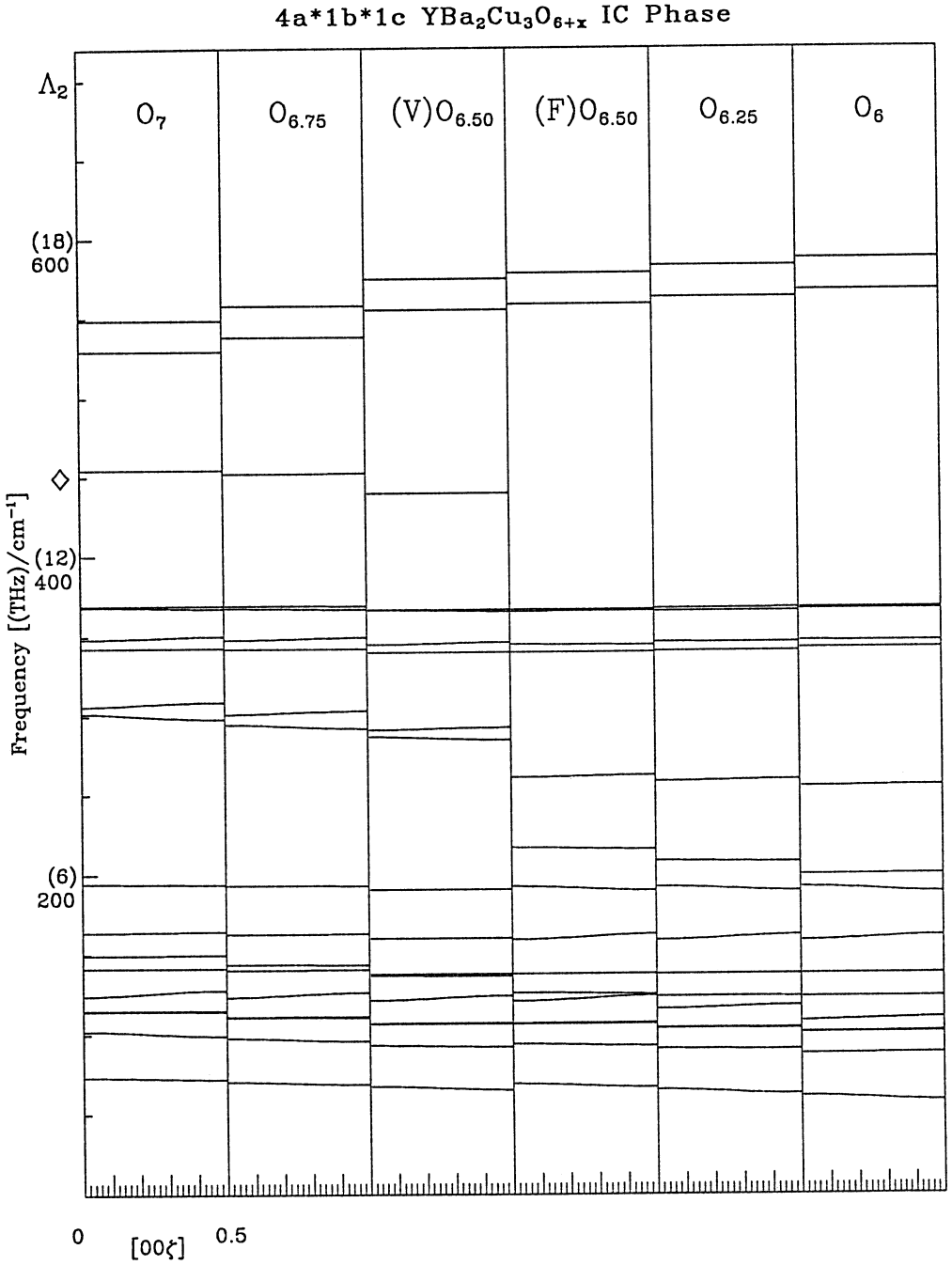


Fig. 5b

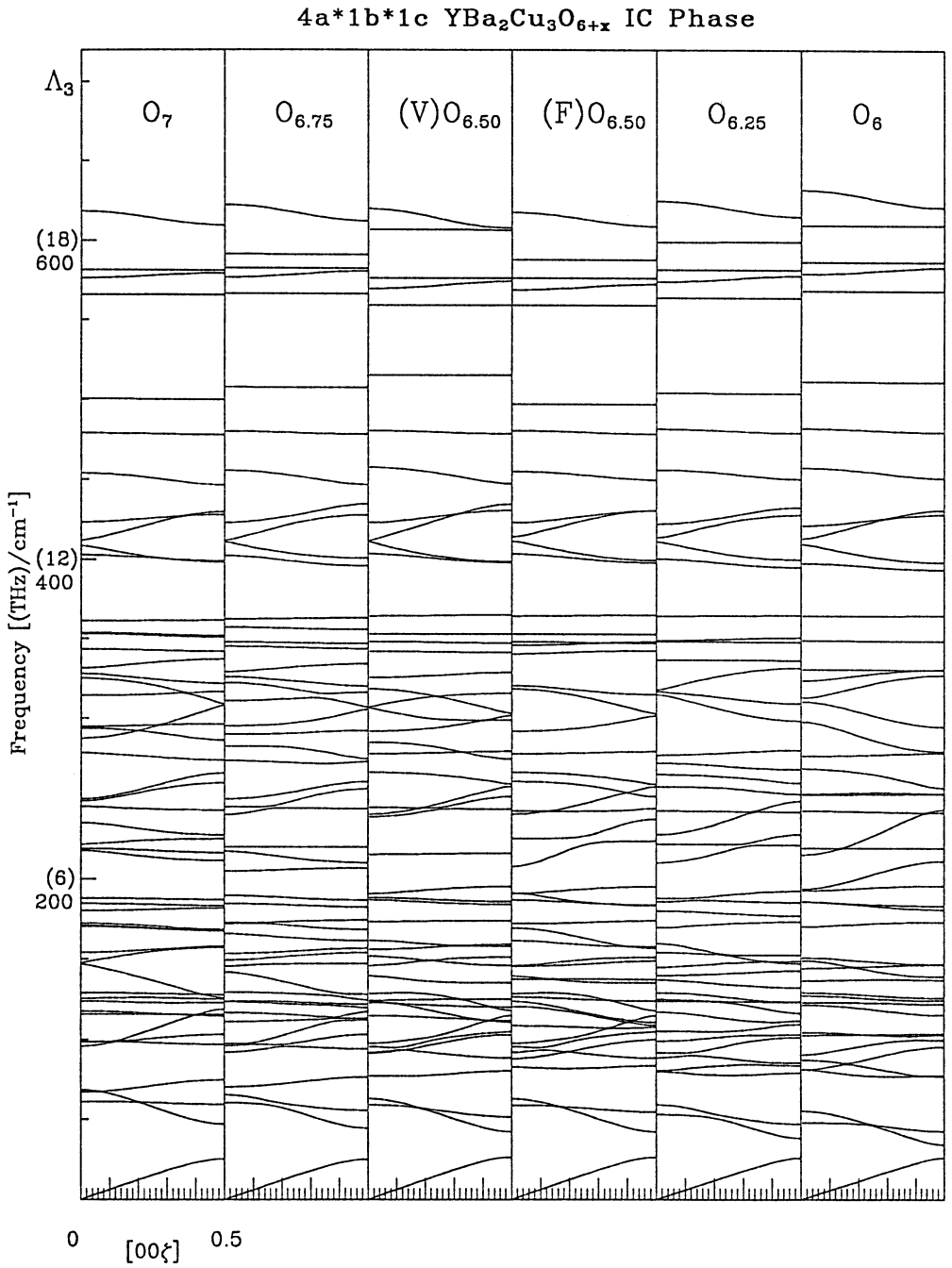


Fig. 5c

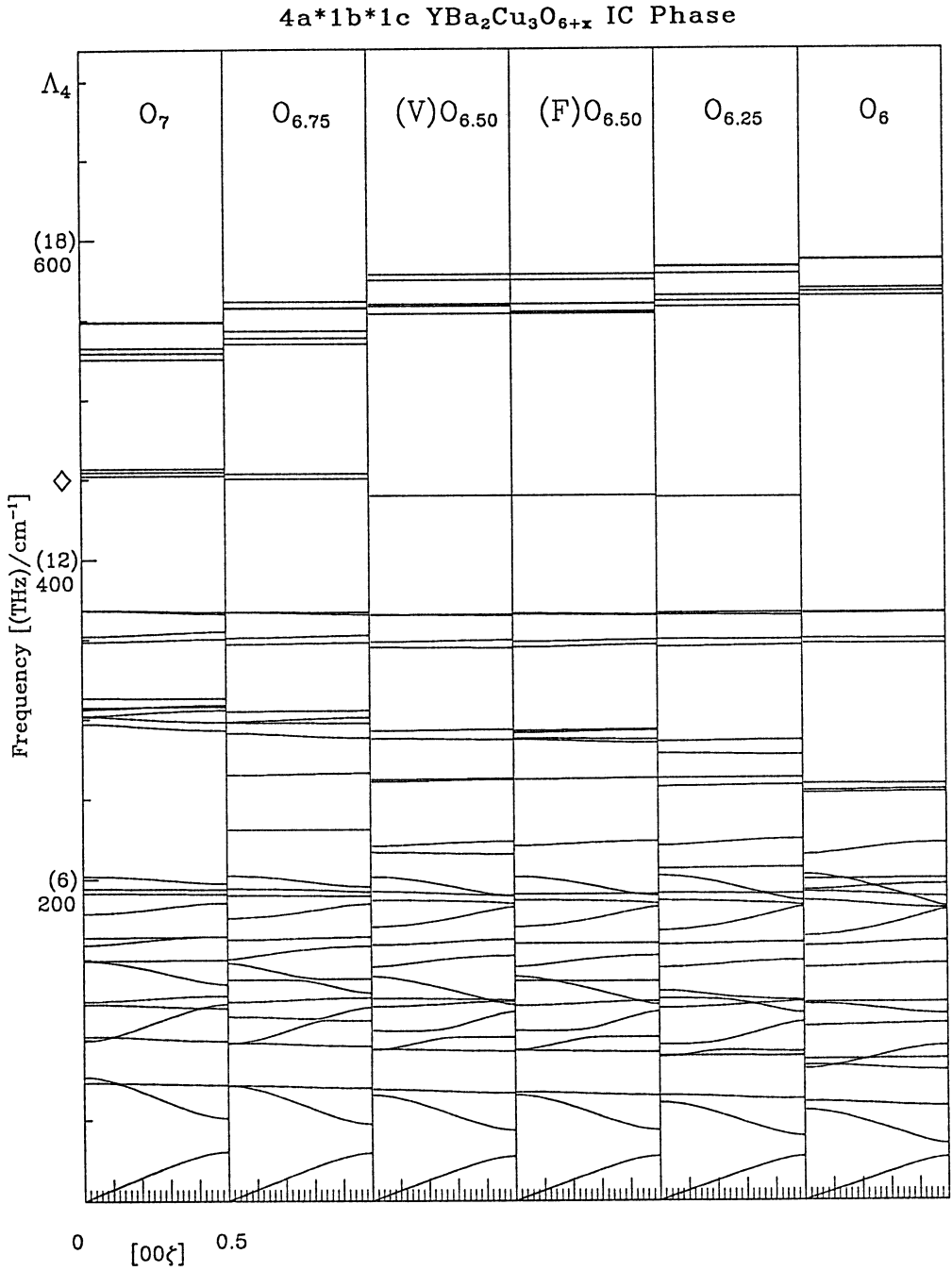


Fig. 5d

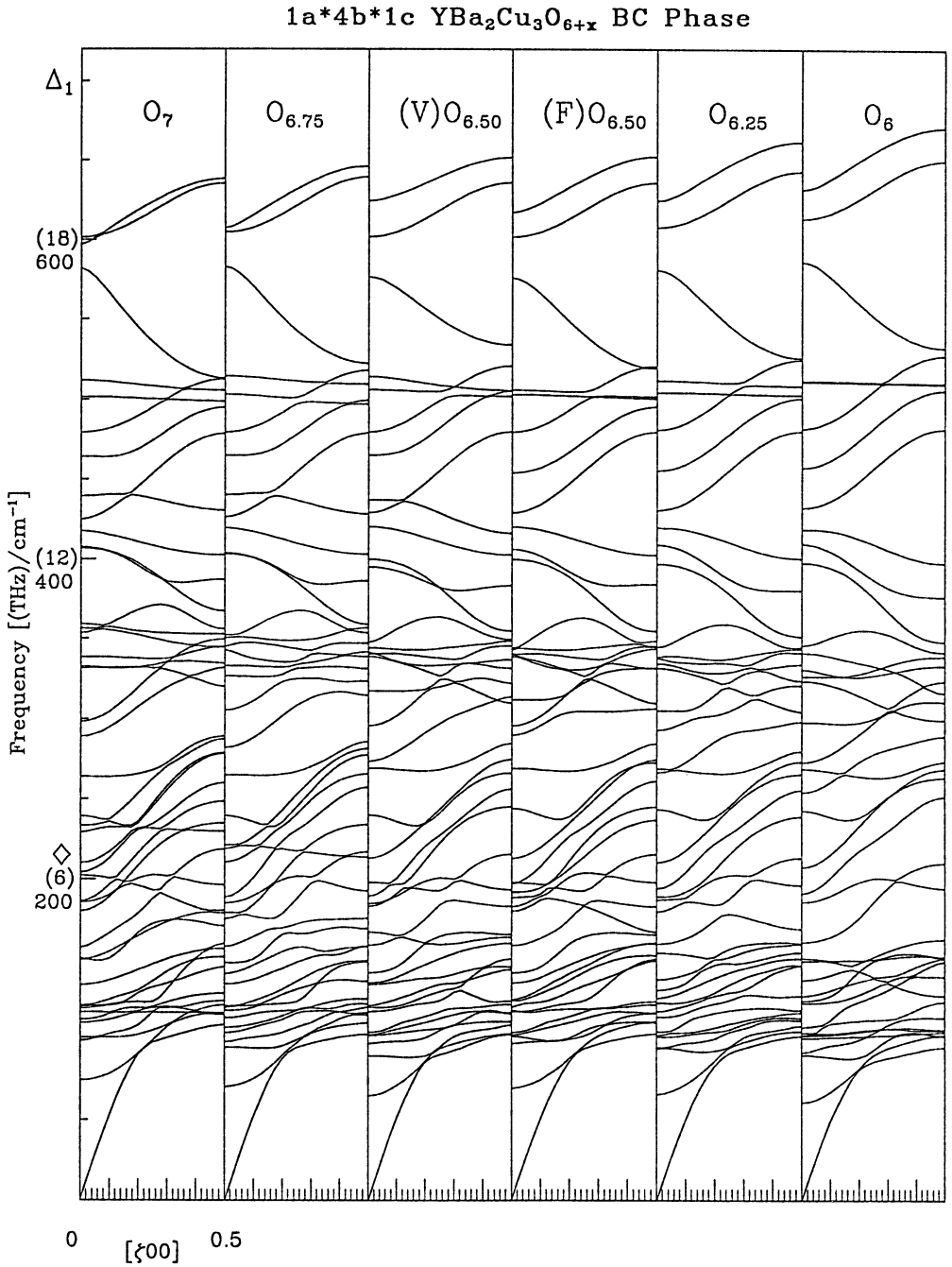


Fig. 6. Dispersion curves of $\text{YBa}_2\text{Cu}_3\text{O}_{6+x}$ for BC phase with q in the $[100]$ direction. The diamond indicates the disappearance of branches.

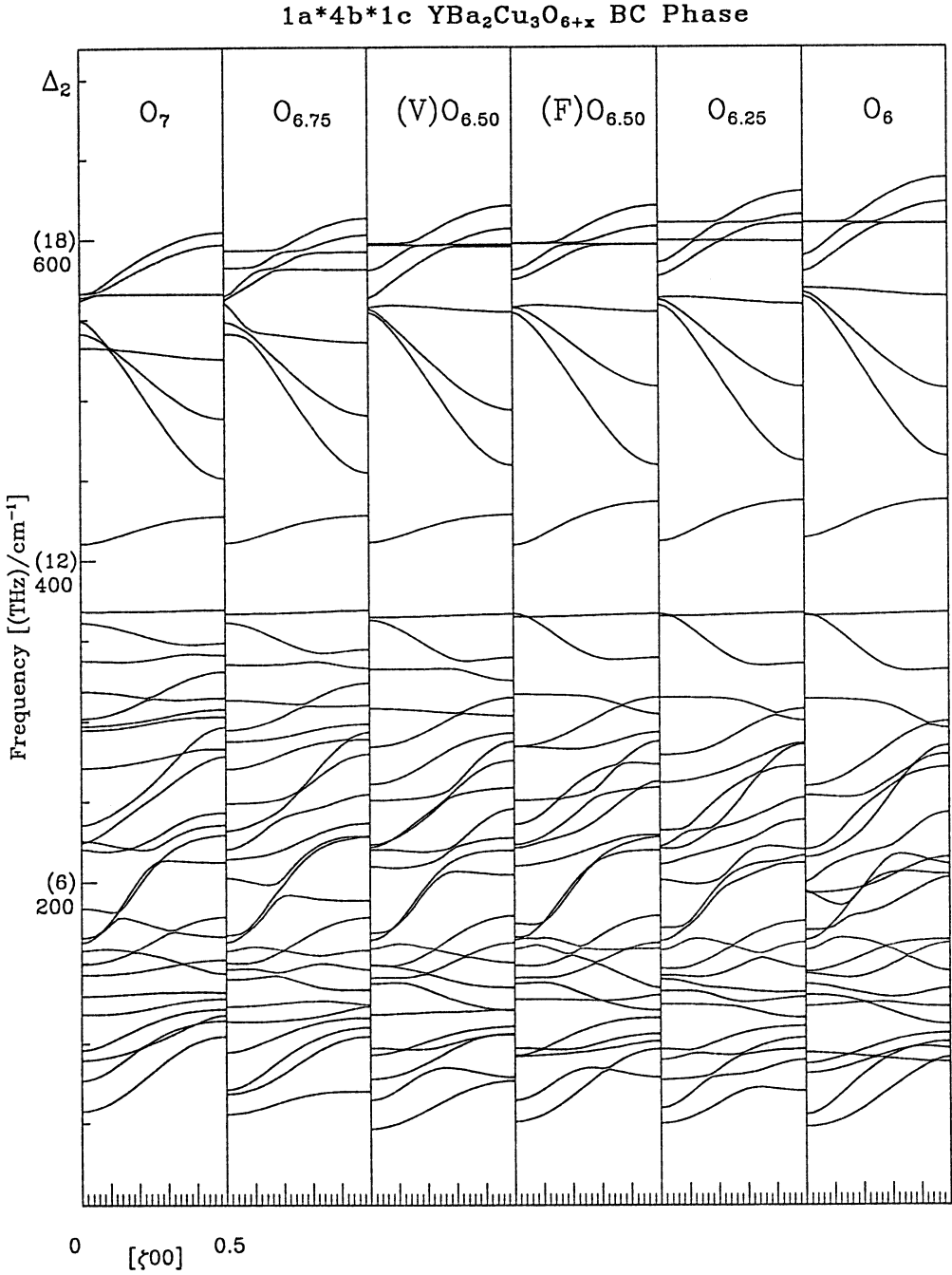


Fig. 6b

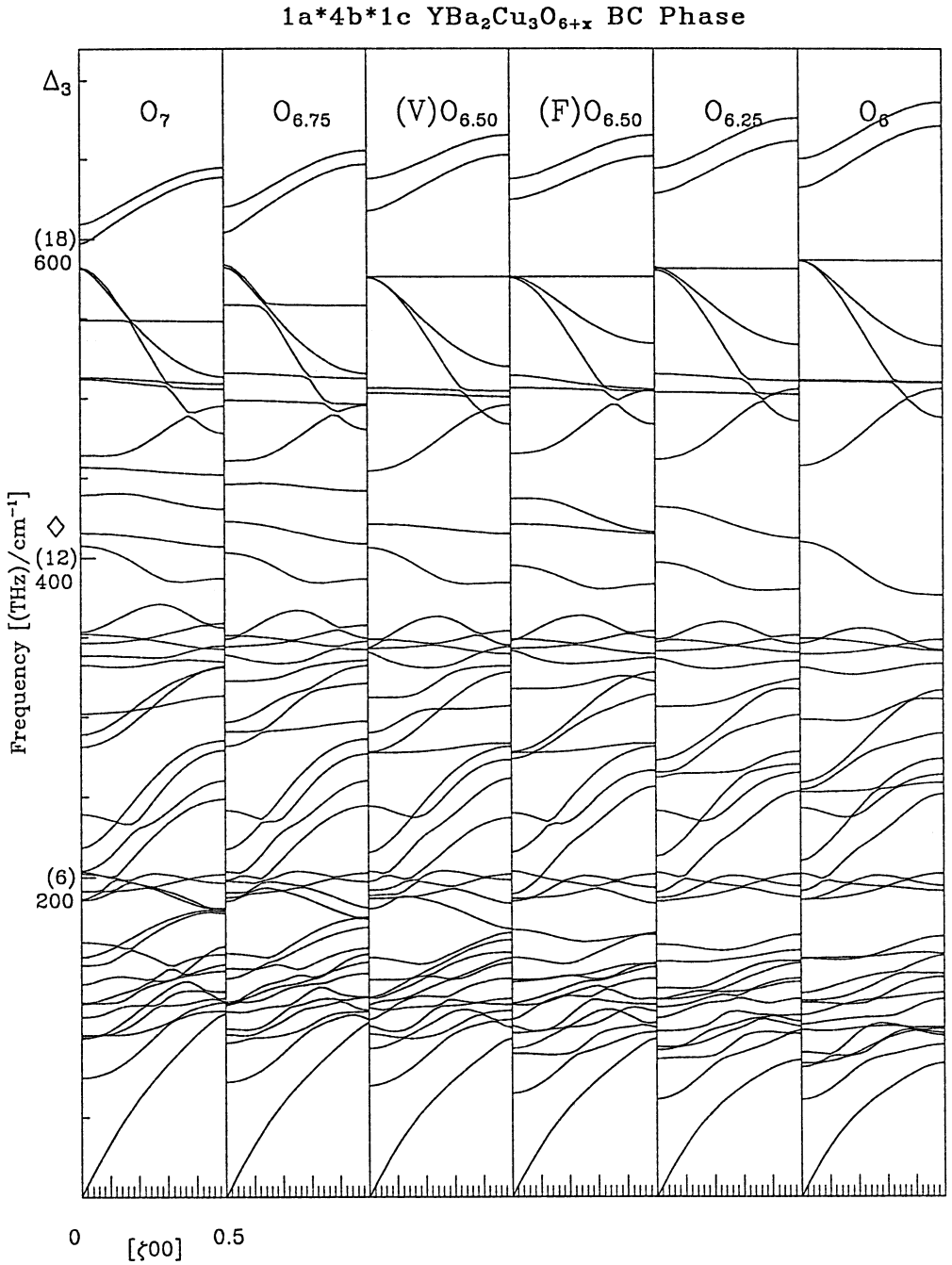


Fig. 6c

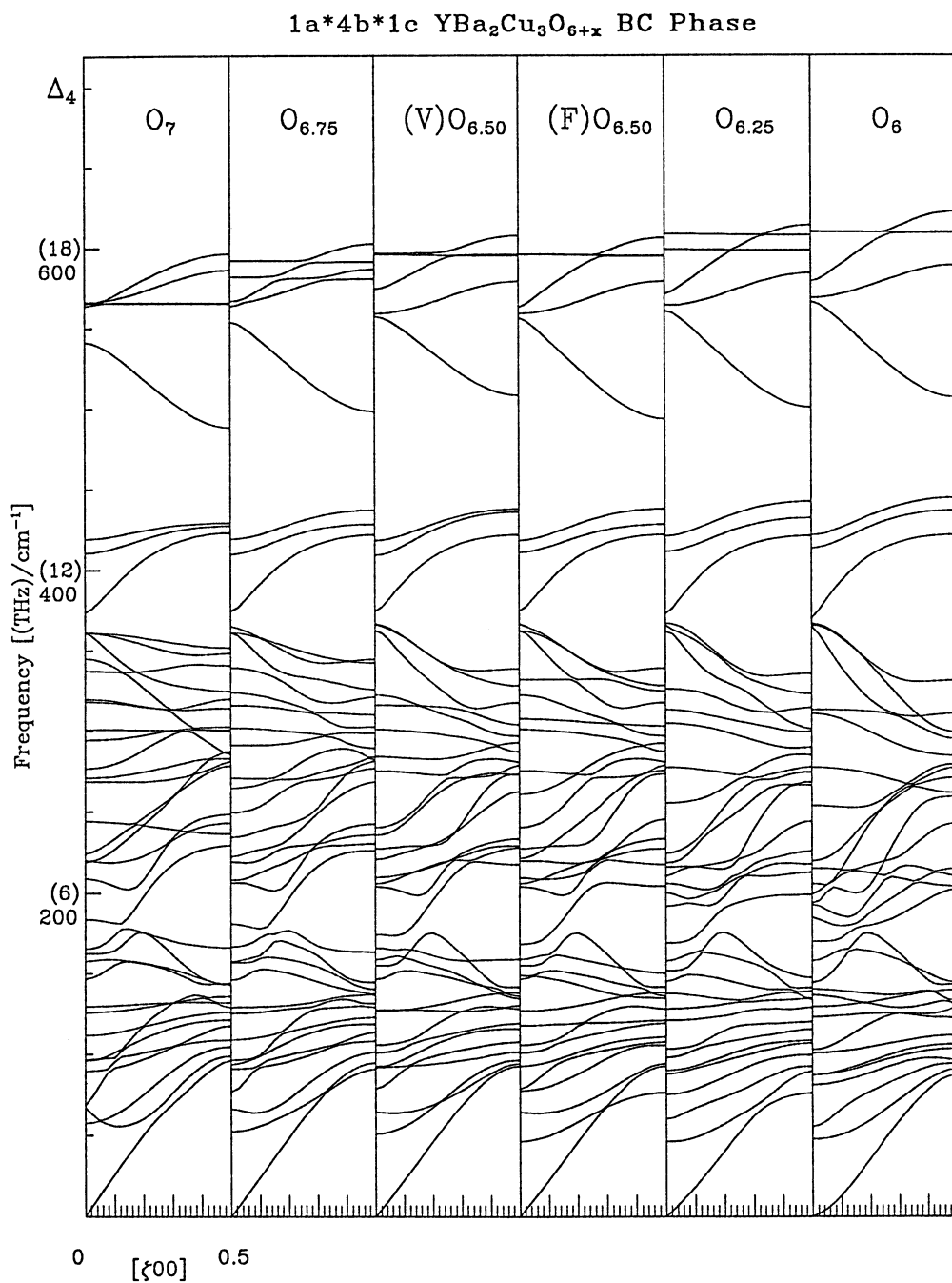


Fig. 6d

Because of the large number and complex structure of the phonon dispersion branches it is difficult to draw conclusions from Figs 3–6. However, the following overall features can be observed.

- (1) The high-energy modes at ~ 19 THz (~ 600 cm^{-1}) generally show a hardening with the removal of oxygen.
- (2) The modes at 10.5 THz (~ 350 cm^{-1}) show a softening with the removal of oxygen.
- (3) For most branches the overall frequency changes are small, but certain modes have significant shifts. Most of the energy shifts are linear with respect to oxygen removal.

In the discussion below we will focus on these points and attempt to give a physical interpretation of the effects.

It should be noted that in general there is no simple one-to-one correspondence between modes for different values of x . Although some modes involve predominantly the motion of one or a few ions, most involve substantial motion of all the ions. Thus as the structure is changed by the removal of oxygen, the character of the modes also changes. One clear instance of this is the disappearance of modes as oxygens are removed. In our supercell calculation three branches are lost at each \mathbf{q} for every removal of one oxygen (corresponding to a decrease of $\Delta x = 0.25$).

We consider the case of \mathbf{q} in the [100] direction of the IC phase shown in Fig. 3. For each change of $\Delta x = 0.25$ one dispersion branch of each symmetry $\Delta_1, \Delta_3, \Delta_4$ vanishes. The regions where these disappearances occur are labelled by the diamond. The simplest case is the group of Δ_3 branches at ~ 13.5 THz (~ 450 cm^{-1}), which are well separated from other modes of the same symmetry. These modes involve predominantly motion of the O(4) ions (the chain oxygens) in the direction of the chain (the \mathbf{b} direction) with some counter motion of the Cu(1) and O(1) ions. In Fig. 7 we show the atomic displacement of this CuO_4 group for all these modes at the point $\mathbf{q} = 0$. For $\text{YBa}_2\text{Cu}_3\text{O}_7$ (column 1) the four modes originate from a single branch of the conventional Brillouin zone. The highest frequency mode is a true $\mathbf{q} = 0$ mode with neighbouring chains vibrating in phase. The two degenerate modes come from $\mathbf{q} = (\pm\frac{1}{4}, 0, 0)$ in the conventional zone and thus have a phase difference of $\pi/2$ between neighbouring chains. In Fig. 7 we show a particular choice for these two—other linear combinations of them are equally valid. The lowest mode comes from the zone boundary $\mathbf{q} = (\frac{1}{2}, 0, 0)$ in the conventional zone and thus has a phase difference of π between adjacent chains.

When one oxygen is removed from the supercell to form $\text{YBa}_2\text{Cu}_3\text{O}_{6.75}$ the supercell becomes the primitive unit cell of the structure. Folding of the Brillouin zone no longer exists and the degeneracies are lifted (see Fig. 7). The vanishing of one of the modes (e.g. Fig. 3c) can be understood physically in the following way. The four modes of the $\text{YBa}_2\text{Cu}_3\text{O}_7$ structure are almost degenerate. Thus, to a good approximation, linear combinations of these will also be stable modes, in particular, one in which the oxygen to be removed is vibrating while the other three are stationary. It is this mode which vanishes. The remaining three modes are shown in the second column of Fig. 7. These are now true $\mathbf{q} = 0$ modes. As can be seen, the highest mode has the three remaining chains vibrating in phase, the intermediate mode has the outside chains in anti-phase and the central chain stationary, and the lowest mode has the outside chains in phase with the central

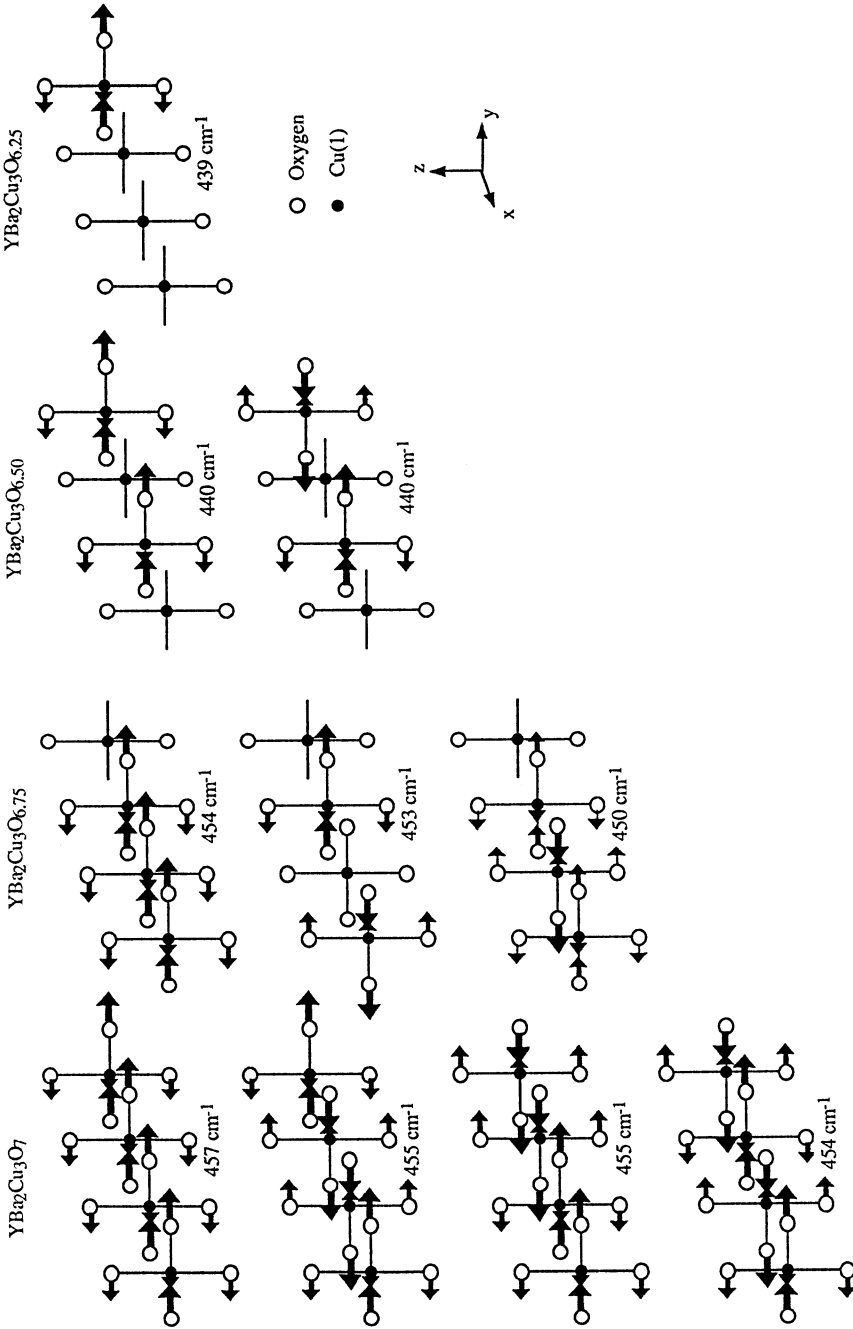


Fig. 7. Atomic vibrations of the vanishing modes of Δ_3 symmetry for different oxygen contents. Only the chain section of the unit cell is shown.

chain in anti-phase with a larger amplitude. At first sight one might expect the order of frequencies to be reversed. It is presumably the influence of the Coulomb interactions which results in the observed order.

When another oxygen is removed to give the $\text{YBa}_2\text{Cu}_3\text{O}_{6.5}$ structure, another mode vanishes. This is essentially a linear combination of the highest and lowest of the $\text{YBa}_2\text{Cu}_3\text{O}_{6.5}$ modes. The remaining two modes (in column 3) are actually the zone-centre mode [O(4) in-phase] and zone-boundary mode [O(4) out-of-phase] of a two-cell supercell which for this structure ($\text{YBa}_2\text{Cu}_3\text{O}_{6.5}$) is the primitive unit cell. The two oxygens are at equivalent sites and thus have the same amplitude. When another oxygen is removed to give the $\text{YBa}_2\text{Cu}_3\text{O}_{6.25}$ structure only one mode remains, and this also vanishes in the $\text{YBa}_2\text{Cu}_3\text{O}_6$ structure. There is an overall softening of this group of modes as oxygens are removed, presumably due to an overall relaxation of the lattice in this region, although this is not obvious. The amplitudes of other atoms also vary with oxygen content, but they are insignificant compared with those of the ions shown in Fig. 7.

The vanishing modes of Δ_1 and Δ_4 symmetry are somewhat more difficult to analyse as they are not well separated from other modes, but possess features similar to those of the Δ_3 modes discussed above. The vanishing of modes in the other directions, labelled by the diamonds in Figs 4–6, can be analysed in a similar way. However, for a \mathbf{q} along [001] in the IC phase (Fig. 5) and for \mathbf{q} along [100] in the BC phase (Fig. 6), because of the different form of folding (see the Appendix), the vanishing branches no longer correspond to the same branch of the conventional Brillouin zone. The symmetries of the modes which vanish vary from case to case, but can always be determined using standard group-theoretical methods.

We now turn to the high-frequency modes. The Δ_1 modes in both the IC and BC phases (Figs 3a and 6a) involve predominantly the vibrations of the O(2) ions in the x direction. In the first case (Fig. 3a) the four highest branches originate from the same branch in the conventional Brillouin zone. In the other case (Fig. 6a) there are two highest branches which originate from different parts of the conventional Brillouin zone. These harden as oxygens are removed from the chains. The same effect is seen in the highest Δ_2 and Δ_3 modes (Figs 3b, 3c, 6b and 6c). These modes involve predominantly the vibrations of O(3) in the y direction. Similar effects on these planar oxygen modes can be seen for \mathbf{q} in the y and z directions (Figs 4 and 5). This hardening of the planar oxygen modes happens despite having oxygens removed from the chain rather than the plane. This suggests that the hardening must be a consequence of the long-range Coulomb interactions between the oxygen ions rather than the short-range interactions, because the chain and the plane are situated far apart. In reality this has been observed (Reichardt 1990; Pintschovius 1990; Pintschovius *et al.* 1991) for the limiting structures ($x = 0, 1$). This hardening is also observed in other Cu–O-based high- T_c superconductors when they are reduced to their semiconducting phases (Reichardt 1990), and may be related to the superconductivity of these Cu–O materials.

However, not all the high-energy planar oxygen modes increase in frequency as the oxygen atoms are removed. The frequencies of the modes of Δ_4 symmetry (Figs 3d and 6d) at ~ 17 THz (~ 570 cm^{-1}), which involve large O(1) amplitudes

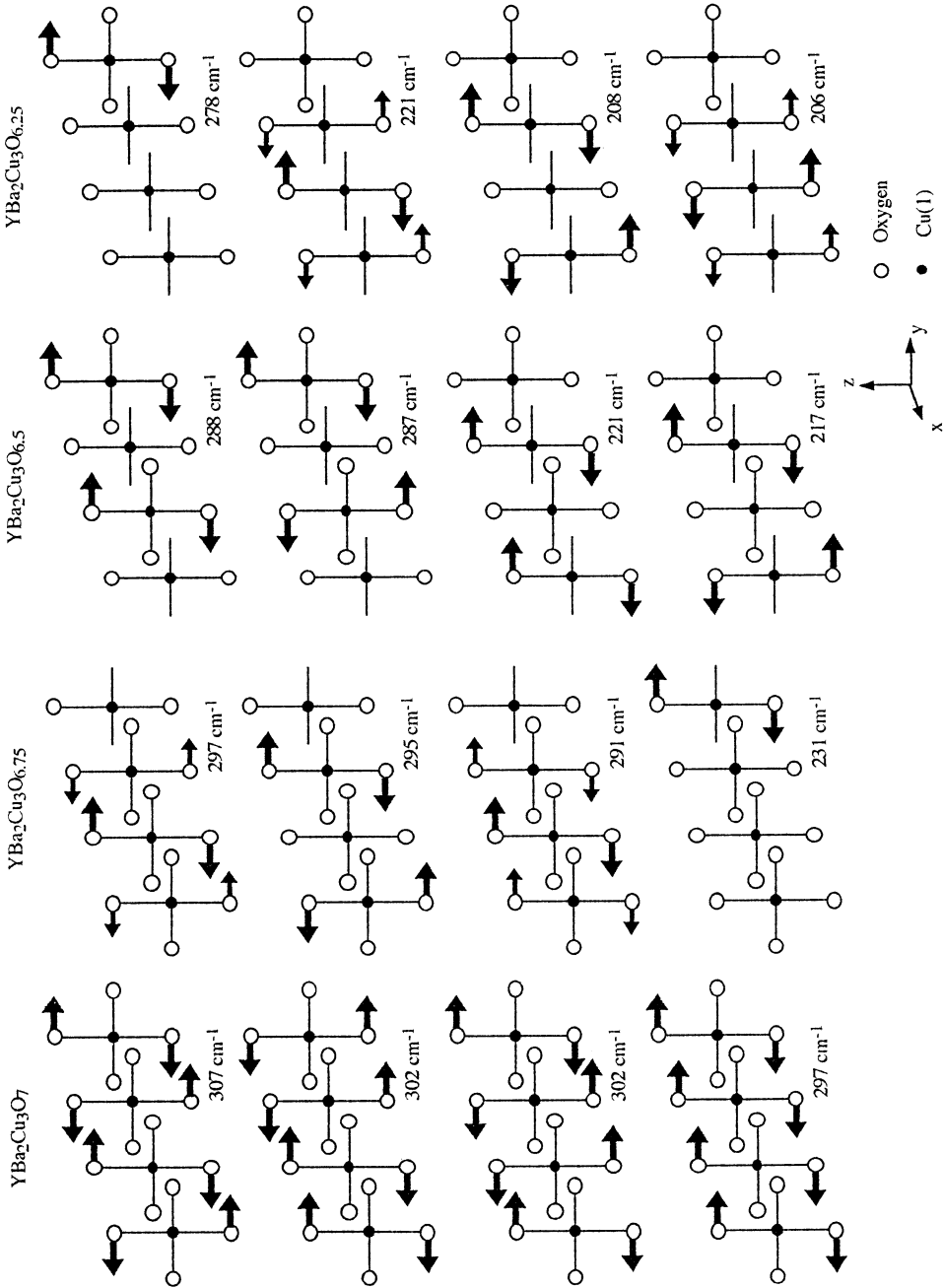


Fig. 8. Atomic vibrations of the shifting modes of Δ_2 symmetry for different oxygen contents. Only the chain section of the unit cell is shown.

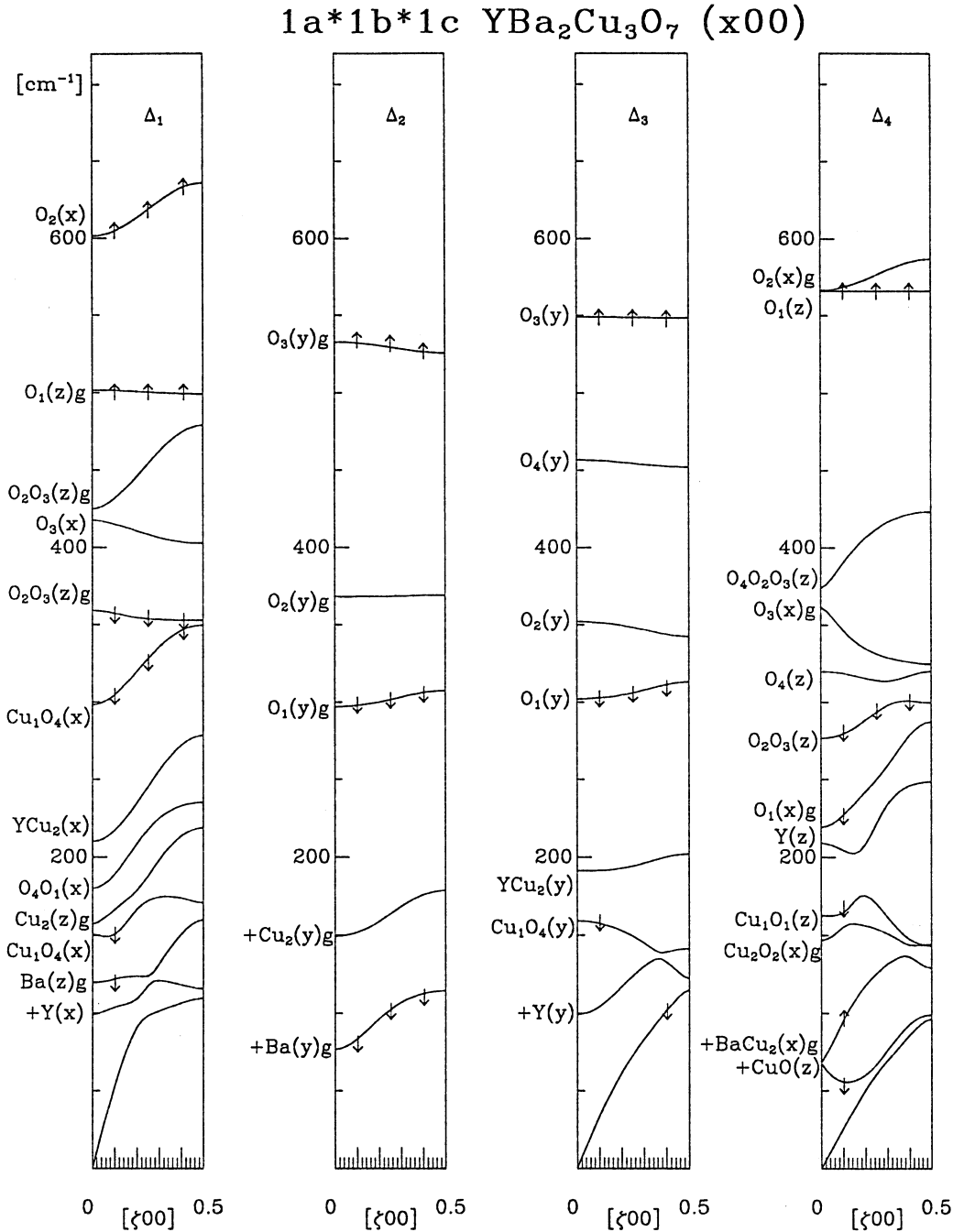


Fig. 9. Changes in dispersion curves of $\text{YBa}_2\text{Cu}_3\text{O}_7$ as oxygen is removed, with q in the x, y, z directions respectively. The arrows indicate the direction of the frequency shifts, and the labels indicate the ion(s) with the largest vibration amplitudes together with the direction of vibration. The symbol $+$ indicates a mode involving significant vibrations of many ions, and the symbol g designates Raman-active modes.

$1a^*1b^*1c$ $\text{YBa}_2\text{Cu}_3\text{O}_7$ ($0y0$)

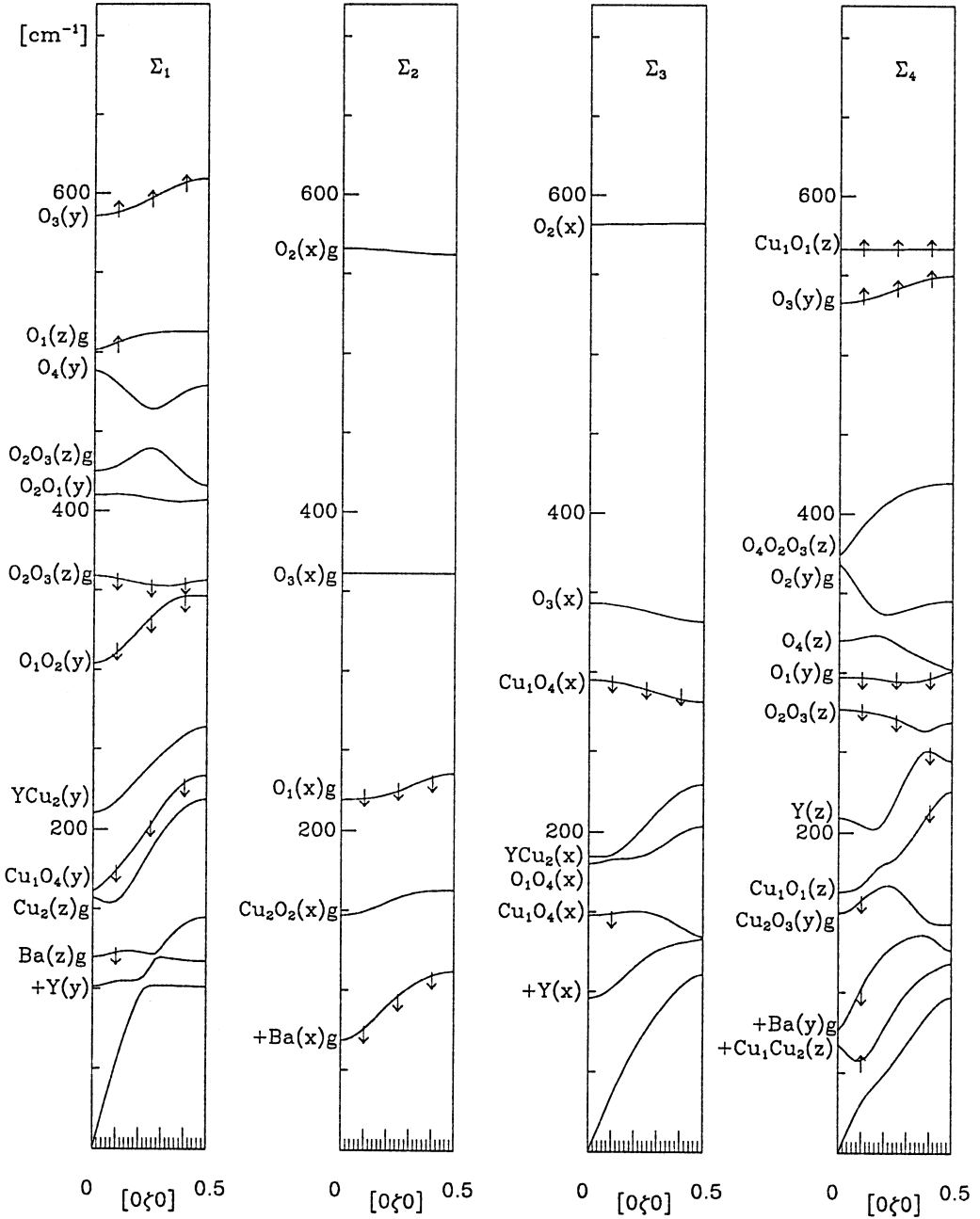


Fig. 9b

1a*1b*1c YBa₂Cu₃O₇ (00z)

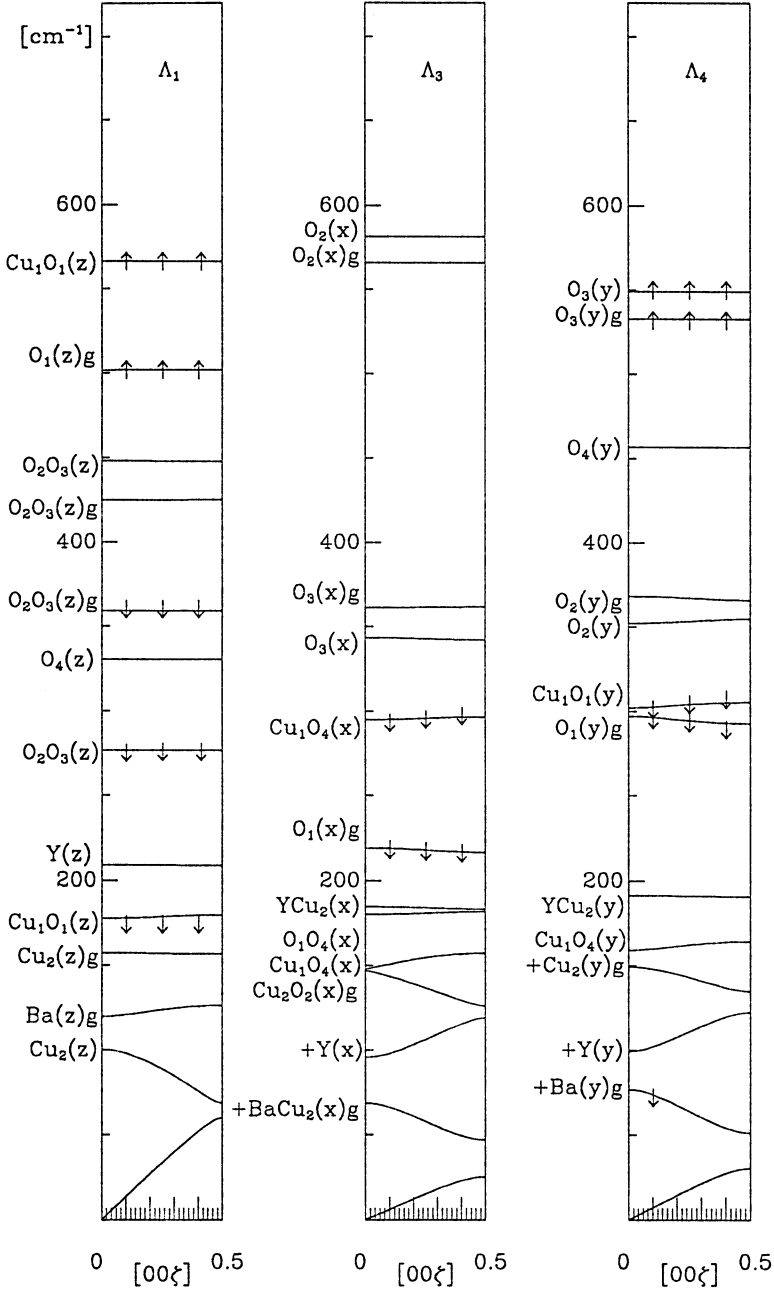


Fig. 9c

in the z direction, increase significantly with oxygen removal but those at the same frequency which involve large O(2) motion change very little. Presumably it is the combination of the changes in the short-range forces, Coulomb forces and the polarisabilities of the ions which bring about the hardening of the former and not the latter modes.

In the medium-energy range $\sim 6.5\text{--}10.5$ THz ($\sim 220\text{--}350$ cm^{-1}), some phonon modes soften significantly (Figs 3*b*, 3*c*, 4*b*, 4*c*, 5*b* and 5*d*). These modes involve predominantly the vibrations of the O(1) and Cu(1) ions. The vibrations of the four Δ_2 modes at ~ 9 THz (~ 300 cm^{-1} , Fig. 3*b* for O_7) are shown in Fig. 8. In this group of modes the Cu(1) ions are stationary while the two neighbouring O(1) ions vibrate in antiphase, in the y direction. The way in which these modes change, on removal of oxygen, can be understood in the same way as for the other groups of modes described above. The softening of these modes is most likely due to the overall softening of this region of the lattice when oxygens are removed.

The response of the phonon modes of $\text{YBa}_2\text{Cu}_3\text{O}_7$ with respect to oxygen removal is summarised in Fig. 9. The phonon branches are labelled according to the ions which have the dominant vibration amplitudes at $\mathbf{q} = 0$. The symbol + in front of a label indicates that the mode is more complex, involving many ions. We should stress however that the vibrational character of a branch will vary continuously with \mathbf{q} , and branches which are close together will also pick up the vibrational character of one another as oxygens are removed. The Raman-active modes are indicated by the symbol g . The other modes are infrared-active. The arrows on these diagrams indicate the dispersion curves which shift significantly in response to oxygen removal.

The phonon density of states (PDS), for both the IC and BC phases, for $x = 0, 0.25, 0.50, 0.75$ and 1.00 , are presented in Fig. 10. They are neutron-weighted (Yim *et al.* 1992). The momentum transfer \mathbf{Q} is taken to be in the range $0 \leq |\mathbf{Q}| \leq 4.4$ \AA^{-1} for all the PDS. One can see a gradual decrease in intensity at medium energy as oxygens are removed. The high-energy peaks in the PDS are also shifted with oxygen removal. These two features are well known in the PDS of $\text{YBa}_2\text{Cu}_3\text{O}_{6+x}$ ($x = 0, 1$) (Renker *et al.* 1988*a*, 1988*b*). The PDS of the stoichiometric materials ($x = 0, 1$) are the same in the IC and BC phases as the structures are identical. The PDS of the non-stoichiometric materials are different in the IC and BC phases, due to the different oxygen orderings in the supercell (see Fig. 2), but the differences between the two phases are small.

4. Conclusion and Summary

In this work we have studied the effects of varying the oxygen concentration on the lattice dynamics of the high-temperature superconducting materials $\text{YBa}_2\text{Cu}_3\text{O}_{6+x}$. Using a supercell approach, which assumes that the O(4) oxygen sites are occupied in a periodic way, we have been able to obtain comprehensive results for the phonon dispersion curves and the phonon densities of states for the five cases $x = 0, 0.25, 0.50, 0.75$ and 1.00 .

Our calculations are based on a simple shell model. The model parameters are adapted from our previous work (Yim *et al.* 1992) on the stoichiometric structures $x = 0, 1$. A systematic interpolation scheme is used to obtain the parameters for

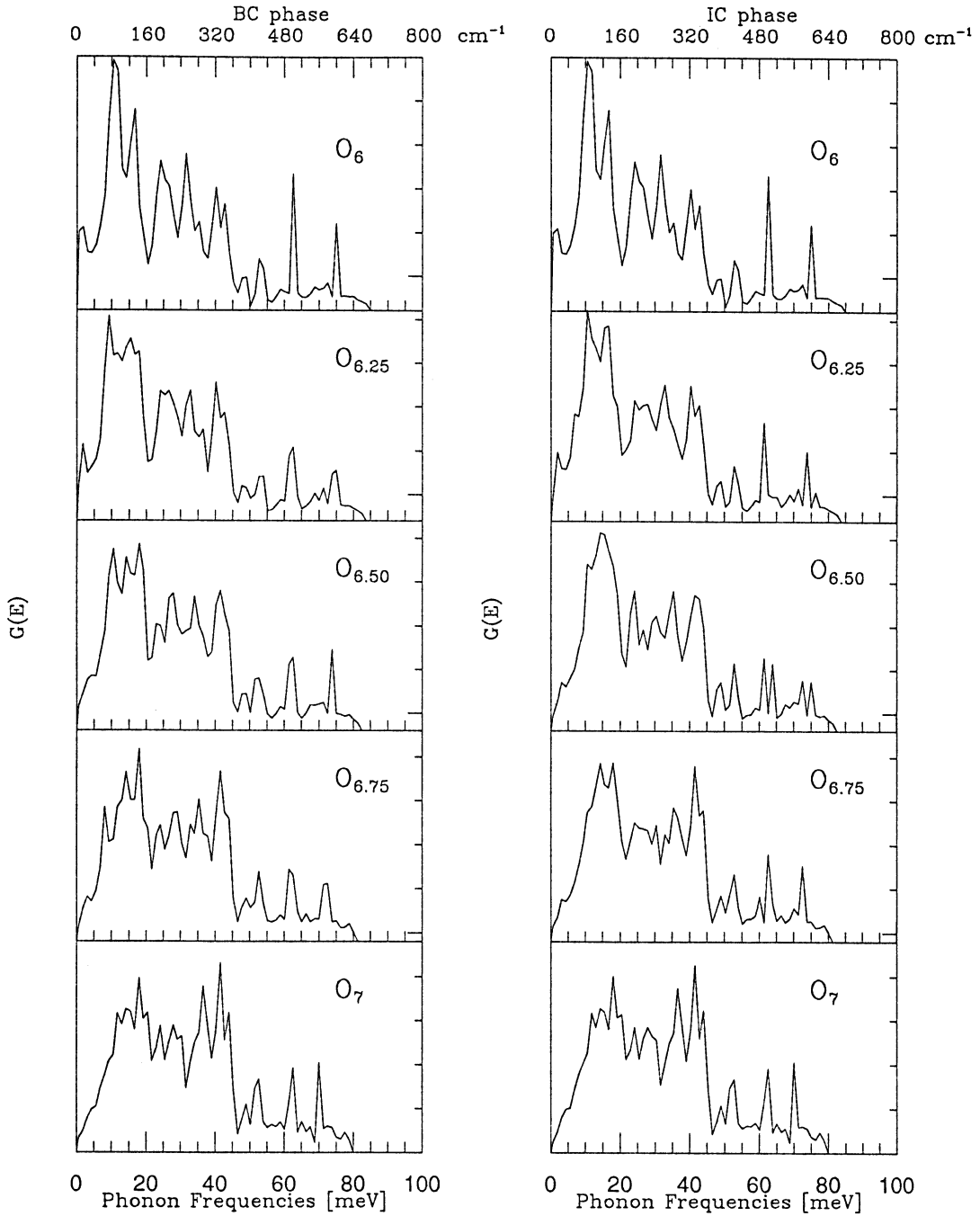


Fig. 10. Phonon density of states of $\text{YBa}_2\text{Cu}_3\text{O}_{6+x}$ for different values of x , for both the BC and IC phases.

the non-stoichiometric cases. In the latter cases we have considered two types of oxygen ordering, where entire chains are removed (IC) and where oxygens are removed identically from all chains (BC). At a temperature below the standard tetragonal-orthorhombic transition the former structure is likely to be the stable one, but it is of interest to see whether the phonon spectra of the two cases have significant differences. In fact the differences are small and so this would not be an effective experimental probe of oxygen ordering.

Because of the complex nature of the phonon spectra of these materials, the changes due to the variation in the oxygen content are also complex, and in general quite small. We have, however, identified several groups of modes where substantial frequency shifts occur. In some cases the modes soften as oxygen is removed, in other cases they harden. We have studied some of these in detail and have presented the form of the dominant atomic motion in these modes. Some tentative explanations for the changes in mode frequencies are proposed. As oxygen is removed the total number of modes decreases. We have identified which modes vanish in this way and have provided a physical picture of the way in which this occurs.

Finally, we comment on the possible comparison with experiment. Direct comparison is difficult since in real samples the distribution of the oxygens will not be periodic as we have assumed. However, we believe that our results should validly predict the observed trends. This is in agreement with the observed results for the limiting cases $x = 0$ and 1. An interesting prediction concerns the number of potentially observable Raman modes. The Raman-active modes are those $\mathbf{q} = 0$ modes which transform as one or more of the symmetric $x_i x_j$ terms. For the stoichiometric materials there are 15 such modes. For the non-stoichiometric materials the number of $\mathbf{q} = 0$ modes increases and hence one might expect these modes will increase in proportion. In practice these modes will not be sharp and may well not be resolvable. However, at low temperature and with good quality samples it may be possible to see the appearance of additional peaks in the Raman spectra, corresponding to these additional modes.

Acknowledgment

One of us (KKY) acknowledges support from the Australian Government through an EMSS scholarship, and support from AINSE through an AINSE Studentship. This work is also partially supported by an ARC grant.

References

- Aligia, A. A., Garces, J., and Bonadeo, H. (1992). *Physica C* **190**, 234.
- Aukrust, T., Novotny, M. A., Rikvold, P. A., and Landau, D. P. (1990). *Phys. Rev. B* **41**, 8772.
- Blumberg, G. E., Fefer, E. M., Fimberg, T., Joon, E., Laht, A., Stern, R., and Rebane, L. A. (1989). *Solid State Commun.* **70**, 647.
- Burdett, J. K. (1992). *Physica C* **191**, 282.
- Burns, G., Dacol, F. H., Feild, C., and Holtzberg, F. (1991). *Solid State Commun.* **77**, 367.
- Cava, R. J., Hewat, A. W., Hewat, E. A., Batlogg, B., Marezio, M., Rabe, K. M., Krajewski, J. J., Peck Jr, W. F., and Rupp Jr, L. W. (1990). *Physica C* **165**, 419.
- Cornwell, J. F. (1971). *Phys. Stat. Sol. B* **43**, 763.
- Crawford, M. K., Farneth, W. E., Bordia, R. K., and McCarron, E. M. III (1988). *Phys. Rev. B* **37**, 3371.
- de Fontaine, D., Wille, L. T., and Moss, S. C. (1987). *Phys. Rev. B* **36**, 5709.

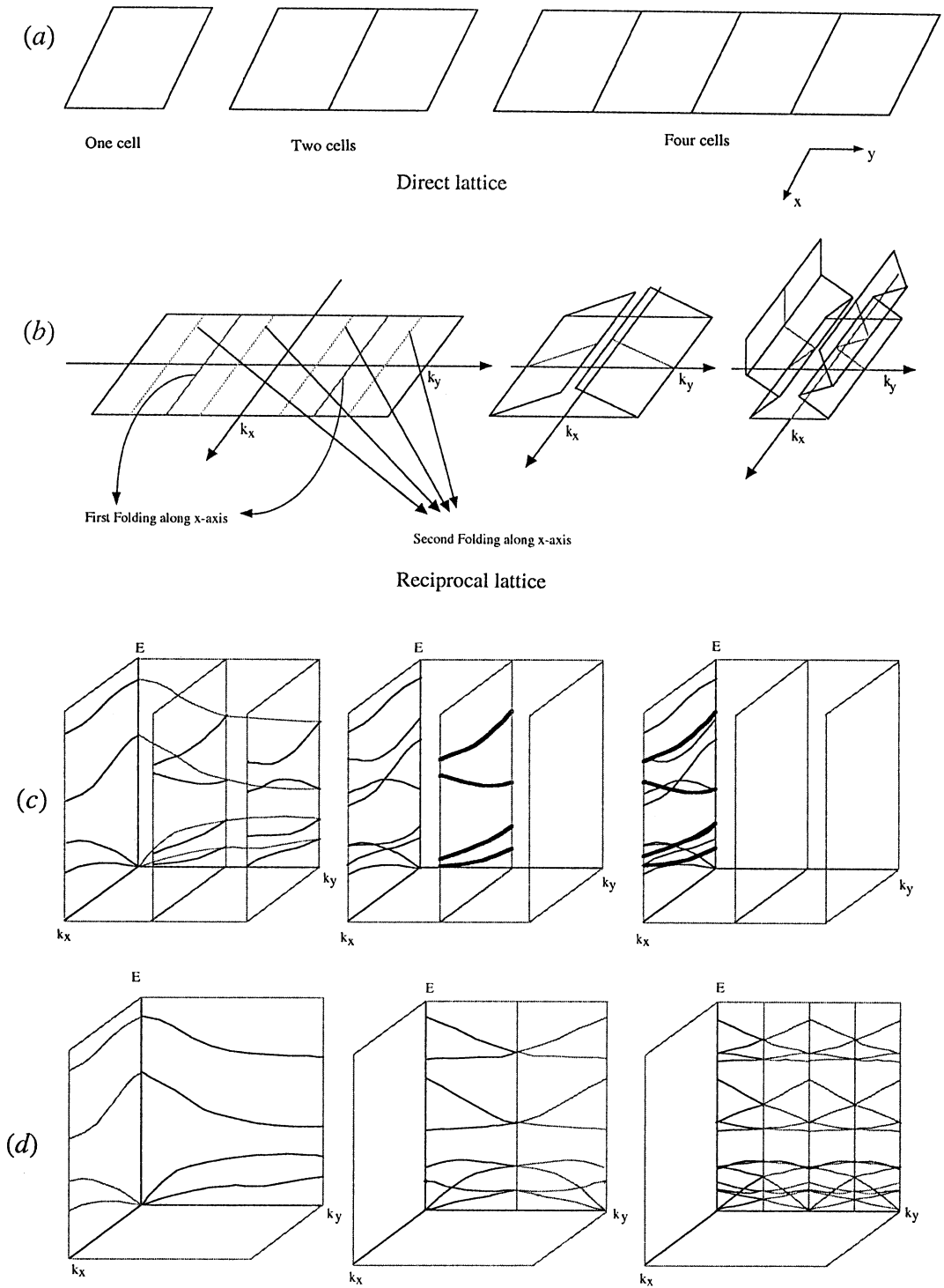


Fig. 11. Expansion of unit cell and corresponding folding of the Brillouin zone (BZ) in a two-dimensional lattice; (a) $1a \times 1b$, $1a \times 2b$ and $1a \times 4b$ unit cells; (b) corresponding BZs, showing the folding transformation; (c) cross-folding, in which dispersion curves from other parts of the BZ are mapped onto the x axis; and (d) self-folding, in which dispersion curves along the y axis are folded into the smaller BZ.

- Echegut, P., Gervais, F., Dembinsky, K., Gervais, M., and Odier, P. (1989). *Solid State Commun.* **69**, 359.
- Feila, R. (1989). *Physica C* **159**, 1.
- Genzel, L., Wittlin, A., Bauer, M., Cardona, M., Schonherr, E., and Simon, A. (1989). *Phys. Rev. B* **40**, 2170.
- Jorgensen, J. D., Veal, B. W., Paulikas, A. P., Nowicki, L. J., Crabtree, G. W., Claus, H., and Kwok, W. K. (1990). *Phys. Rev. B* **41**, 1863.
- Kress, W., Schroder, U., Prade, J., Kulkarnie, A. D., and de Wette, F. W. (1988). *Phys. Rev. B* **38**, 2906.
- McCarty, K. F., Liu, J. Z., Shelton, R. N., and Radosky, H. B. (1990). *Phys. Rev. B* **41**, 8792.
- Morioka, Y., Tokiwa, A., Kikuchi, M., Syono, Y., and Nagase, K. (1989). *Solid State Commun.* **70**, 1127.
- Pintschovius, L. (1990). *Festkorperprobleme (Adv. Solid State Phys.)* **30**, 183.
- Pintschovius, L., Pyka, N., Reichardt, W., Rumiantsev, A., Mitrofanov, N. L., Ivanov, A. S., Collin, G., and Bourges, P. (1991). *Physica C* **185-9**, 156.
- Reichardt, W. (1990). *Neutron News* **1**, 20.
- Renker, B., Gompf, F., Gering, E., Roth, G., Reichardt, W., Ewert, D., Rietschel, H., and Mutka, H. (1988a). *Z. Phys. B* **71**, 437.
- Renker, B., Gompf, F., Gering, E., Ewert, D., Rietschel, H., and Dianoux, A. J. (1988b). *Z. Phys. B* **73**, 309.
- Van Tendeloo, G., Zandbergen, H. W., and Amelinckx, S. (1987). *Solid State Commun.* **63**, 603.
- Yasuda, T., and Mase, S. (1989). *J. Phys. Soc. Jpn* **58**, 195.
- Yim, K. K., Oitmaa, J., and Elcombe, M. M. (1992). *Aust. J. Phys.* **45**, 221.
- Zeiske, Th., Hohlwein, D., Sonntag, R., Kubanek, F., and Collin, G. (1992). *Z. Phys. B* **86**, 11.

Appendix

We briefly describe the transformation of the Brillouin zone which occurs when the size of the unit cell is increased. This is most easily shown by a simple two-dimensional rectangular structure (Fig. 11). In this figure the supercell is expanding along the y direction. One can notice that there are two types of folding of the dispersion curves. For dispersion curves along the direction of expansion, *viz.* the y axis, the curves are folded onto themselves; this we refer to as self-folding. Along the x axis, dispersion curves from the zone boundary are folded onto the existing dispersion curves on that axis. We refer to this as cross-folding.

In the $\text{YBa}_2\text{Cu}_3\text{O}_{6+x}$ ($x = 0, 1$) system, a $(1a \times 4b \times 1c)$ supercell is used for the BC phase, resulting in a $(1k_a \times 0.25k_b \times 1k_c)$ Brillouin zone. The dispersion curves along the k_b axis are self-folded onto themselves twice. In the IC phase the supercell $(4a \times 1b \times 1c)$ is used and hence the Brillouin zone is of dimensions $(0.25k_a \times 1k_b \times 1k_c)$. Here it is the dispersion curves along the k_a axis which are self-folded onto themselves twice. For other symmetry axes the cross-folding is as follows:

Axes	BC phase	IC phase
k_a	$\{(k_a, m/4, 0) \ m = 0, 1, 1, 2\}$	Self folding
k_b	Self-folding	$\{(m/4, k_b, 0) \ m = 0, 1, 1, 2\}$
k_c	$\{(0, m/4, k_c) \ m = 0, 1, 1, 2\}$	$\{(m/4, 0, k_c) \ m = 0, 1, 1, 2\}$

In each case the dispersion curves on the $m = 1$ lines are doubly degenerate.

